Hierarchically porous carbon foams coated with carbon nitride: Insights into adsorbents for pre-combustion and post-combustion CO_2 separation

Maryna Vorokhta[a,b*], Muhammad Irfan Maulana Kusdhany[c], Martina Švábová[a], Masamichi Nishihara[b,c,d], Kazunari Sasaki[b,d,e], Stephen Matthew Lyth[b,f,g*]

[a]*Department of Geochemistry, Institute of Rock Structure and Mechanics, Czech Academy of Sciences, V Holešovičkách 94/41, 18209 Prague 8, Czech Republic*

[b]*Next-Generation Fuel Cell Research Center (NEXT-FC), Kyushu University, 744 Motooka, Nishi-ku, Fukuoka, 819-0395, Japan*

[c]*Department of Automotive Science, Graduate School of Integrated Frontier Sciences, Kyushu University, 744 Motooka, Nishi-ku, Fukuoka, 819-0395, Japan*

[d]*International Research Center for Hydrogen Energy, Kyushu University, 744 Motooka, Nishi-ku, Fukuoka, 819-0395, Japan*

[e]*Department of Hydrogen Energy Systems, Faculty of Engineering, Kyushu University, 744 Motooka, Nishi-ku, Fukuoka, 819-0395, Japan*

[f]*Department of Chemical and Process Engineering, University of Strathclyde, 75 Montrose St, Glasgow G1 1XL, United Kingdom*

[g]*Department of Mechanical Engineering, University of Sheffield, Western Bank, Sheffield, S10 2TN, United Kingdom*

*Corresponding Author. E-mail address: vorokhta@irsm.cas.cz (M. Vorokhta), stephen.lyth@strath.ac.uk (S.M. Lyth)

Abstract

Adsorption is fundamental to many industrial processes, including separation of carbon dioxide from other gases in pre- or post-combustion gas mixtures. Adsorbents should have high capacity and selectivity, which are both intimately linked with surface area, pore size distribution, and surface energy. Porous carbons are cheap and scalable adsorbents, but greater understanding of how their textural properties and surface chemistry affects their performance is needed. Here, we investigate the effect of nitrogen doping on CO_2 adsorption. Microporous carbon foams with large surface area (> 2500 m^2 g^{-1}) and pore volume (1.6 cm^3 g^{-1}) are synthesized, then coated with varying amounts of carbon nitride (up to 17 at% nitrogen) to achieve high CO_2 uptake (25.5 mmol g^{-1}) and selectivity (CO_2:N_2 = 21), whilst also giving insights into the relationship between structure and function. At low pressure (relevant to post-combustion capture), moderate carbon nitride loading leads to enhanced uptake and selectivity by combining large ultramicropore volume with the introduction of Lewis base sites, leading to high isosteric heat of adsorption. Higher carbon nitride loading further increases selectivity but lowers uptake by blocking micropores. Conversely, at high pressure (relevant to pre-combustion capture) the uncoated carbon foam displays superior uptake, because mesoporosity is the dominant factor in this regime, rather than the presence of ultramicropores. Finally, the samples displayed excellent regeneration under repeated adsorption-desorption cycles, and breakthrough curves were measured. These results underscore the delicate balance required for optimal material design when applying porous carbon adsorbents to CO_2 separation processes. Moving forward, improved adsorbents will contribute to the proliferation of carbon capture and storage (CCS) and carbon capture and utilisation (CCU) technologies, ultimately contributing reduced anthropogenic CO_2 emissions.

Keywords: porous carbons, CCS, CO_2 adsorption, selectivity, breakthrough curve, isosteric heat

1. INTRODUCTION

Anthropogenic CO_2 emissions are contributing to global heating, extreme weather, and ocean acidification [1,2]. Resolving this is crucial to prevent environmental catastrophe. Thermal power plants burning fossil fuels are the main culprit for these emissions, so should be the main target of remediation technologies [3]. Carbon capture utilisation and storage (CCUS) technologies, crucial for the separation of CO_2 from other gases, include pre-combustion, post-combustion, and oxy-fuel combustion capture methods [4].

In the field of gas separation, much research focusses on the design of adsorbent materials tailored for CO_2 capture. Adsorbents must fulfil stringent criteria, including high adsorption capacity, good selectivity, fast kinetics, and efficient regeneration over many adsorption-desorption cycles [5]. Furthermore, the material must be cost-effective and obtained sustainably. As such, porous carbons are widely employed in separation [6–10]. Other materials commonly investigated include metal-organic frameworks (MOFs) [11], carbonyl-based polymers [12], hypercrosslinked polymers (HPCs) [13], zeolites [14,15], cement [16], and silica [17,18]. Machine learning analyses of the extensive data, identify essential adsorbent characteristics for separation, including large pore volume (> 0.5 cm^3 g^{-1}), high specific surface area (> 450 m^2 g^{-1}), and small pore diameter (< 0.442 nm), confirming the suitability of porous carbons [19]. Indeed, activated carbons are thought to be the most-studied class adsorbents for of CO_2 separation in recent years [20].

Despite their widespread application, there is still significant scope for improving the activated carbons for CO_2 separation. Two main strategies involve: (i) maximising the surface area and tailoring the pore volume to increase the adsorption sites within micropores, and (ii) altering the surface chemistry to enhance the adsorbate-adsorbent interactions by inducing hydrogen bonding, dipole-dipole or Lewis acid-base interactions. Varying the porosity can be achieved by controlling the activation conditions. For pre-combustion applications, mesopores are generally beneficial [7,21], whilst for post-capture technologies micropores are targeted [22,23]. Meanwhile, surface chemistry adjustments often involve nitrogen-doping [24,25], introducing Lewis base sites that interact strongly with CO_2, a Lewis acid [26]. Nitrogen incorporation can be achieved by using nitrogen-rich precursors [27], or heating carbons in the presence of nitrogen-rich compounds [28]. However, these techniques often make it challenging to precisely control the nitrogen content or achieve high nitrogen levels.

Coating materials with carbon nitride, with its high nitrogen-to-carbon ratio (4:3), can significantly increase nitrogen content. Graphitic carbon nitride (g-C_3N_4) can be formed by the condensation of melem into tri-s-triazine subunits, linked by tertiary nitrogen (Scheme S1) [29],

while incomplete polymerisation yields amorphous forms (a-C_3N_4) with variable nitrogen content [30]. Due to the combination of excellent stability, high nitrogen content, and ultramicropores formed between triazine subunits, carbon nitrides have been investigated as CO_2 adsorbents in several cases. For example, carbon nitride aerogels adsorb 4.2 mmol g^{-1} of CO_2 with selectivity of 113 (CO_2/N_2 = 10/90 vol%) at 300 K and 100 kPa [31]; microporous carbon nitrides with uptake of ~6.2 mmol g^{-1} at 273 K and 3 MPa [32], and ordered mesoporous carbon nitrides with uptake of 5.63 mmol g^{-1} at 273 K and 3 MPa [33] have been reported. Meanwhile, templated mesoporous carbon nitrides achieved very high CO_2 uptake of 13.5 mmol g^{-1} at 3 MPa due to their relatively large surface area (901 m^2 g^{-1}) [34]. Most notably, polyethylenimine-functionalized carbon nitrides exhibited exceptional selectivity (>6500 for CO_2/N_2 = 15/85 vol%), albeit with low adsorption capacity (1.8 mmol g^{-1} at 298 K) [35], attributed to strong chemisorption by amine groups reacting with CO_2 [35].

Carbon nitride coating exhibits a different mechanism in CO_2 adsorption compared to nitrogen doping. Accordingly, nitrogen doping integrates nitrogen atoms into the carbon material lattice, creating defects and altering electronic properties of the carbon framework. This enhances the carbon surface basicity and improves CO_2 uptake, as nitrogen atoms acting as Lewis bases readily interact with acidic CO_2 [28]. Conversely, carbon nitride does not integrate into the carbon framework but rather coats the material, primarily adsorbing CO_2 through interactions with its nitrogen-containing units. The high CO_2 adsorption of carbon nitrides is mainly due to abundant amine groups [34]. Additionally, CO_2 adsorption occurs on the polarised micropore edges formed by the surface roughness of graphitic carbon nitride, exposing electron-rich edges towards CO_2 through induced dipole-dipole interactions, while tertiary nitrogen and heptazine sites exhibit very weak or no polarisation effect on CO_2 [31]. When analysing the mechanism of CO_2 adsorption on different nitrogen functional groups, adsorption energy studies showed that quaternary nitrogen and pyrrolic nitrogen enhance surface CO_2 adsorption, while pyridine nitrogen enhances edge CO_2 adsorption [36].

We previously reported CO_2 adsorption on carbon foams (synthesized from sodium ethoxide) and nitrogen-doped carbon foams (ethanolamines as nitrogen sources), having hierarchical porosity with large micropore volume, resulting in remarkable surface area up to 3450 m^2 g^{-1} [37,38]. We reported CO_2 uptake of up to 5.65 mmol g^{-1} at 100 kPa, and 9.88 mmol g^{-1} at 0.5 MPa, and at 298 K [37], making them extremely promising adsorbents. We showed that selectivity was dependent on nitrogen content, but capacity decreased with nitrogen content due to reduced pore volume [28]. Therefore, further optimization is still required to find a balance between pore volume and nitrogen content.

The aim of this study is to gain insights into the performance of carbon foam adsorbents for CO_2 capture by increasing nitrogen content without destroying the carbon foam framework. This is achieved by synthesizing carbon nitride on the surface of carbon foams, via polymerisation of dicyandiamide. Furthermore, we investigate the suitability of the materials for both pre-combustion (2 MPa) and post-combustion (100 kPa) scenarios at different temperatures, under dynamic CO_2/N_2 gas mixture conditions in a packed bed, and across multiple adsorption-desorption cycles. This approach to industrial adsorbent design promises not only to improve efficiency but also enhance sustainability, marking significant steps toward mitigation of the impending environmental crisis.

2. EXPERIMENTAL

2.1 Synthesis of carbon nitride-coated carbon foams

All chemicals were used as received without further purification. Microporous carbon foam (CF) was prepared via a single-step pyrolysis of sodium ethoxide (Wako Ltd., Japan) in a muffle furnace at 973 K with a ramp rate of 3 K min^{-1} and under a flowing nitrogen atmosphere (6 L min^{-1}). This high flow rate was necessary due to the large internal volume of the muffle furnace in order to prepare a substantial amount of CF for subsequent coating with carbon nitride. For the CF preparation, we used about 35 g of sodium ethoxide. The resulting product was crushed in a pestle and then magnetically stirred in deionised water for at least 24 hours, followed by vacuum filtration and washing until the filtrate had neutral pH, to remove soluble by-products such as sodium carbonate and sodium hydroxide [37]. The product was then dried for 24 hours at 333 K. The carbonaceous product yield was 1.95 g, making up 5.6 % of the initial mass of sodium ethoxide.

A portion of the CF of about 500 mg was then coated with carbon nitride. This was achieved via wet impregnation with dicyandiamide (DCD, Wako Ltd., Japan). DCD was dissolved in deionized water, and CF powder was added to the solution with a DCD:CF ratio of 1:2 wt/wt. The resulting dispersion was magnetically stirred at 500 rpm for either 1 hour or for 24 hours as a means to control the nitrogen content. Then the water was evaporated overnight in an oven at 333 K. The dried DCD-coated CF samples were then subjected to two-step heat treatment in a tube-furnace to polymerise the DCD into carbon nitride, first at 823 K for 4 hours (with a ramp rate of 3 K min^{-1}), then at 973 K for 2 hours, both steps carried out

under flowing nitrogen gas at 100 ml min^{-1}. The resulting samples were labelled as C_3N_4/CF-1 and C_3N_4/CF-24, reflecting the different durations of the wet impregnation step.

2.2 Characterization methods

The morphology of the samples was studied by scanning electron microscopy (SEM, SU-9000 microscope, Hitachi Ltd., Japan). The particle size distribution, based on the length of the particles observed in the SEM images, was determined using ImageJ software. It should be noted that as the particles were non-uniform, the length of each respective particle was measured and given as the size parameter. Surface chemical composition was determined under ultra-high vacuum via X-ray photoelectron spectroscopy (XPS, PHI 5000 VersaProbe-II Focus Microprobe, ULVAC-PHI Ltd., Japan). The bulk chemical composition was estimated by CHN elemental analysis (CHN Corder MT-6, Yanaco Apparatus Development Laboratory Co. Ltd., Japan). Crystallinity was investigated via powder X-ray diffraction (XRD, SmartLab diffractometer, Rigaku Ltd., Japan) and Raman microscopy with an excitation wavelength of 534 nm (inVia Raman microscope, Renishaw Ltd., Japan). Deconvolution of the Raman spectra to obtain the areas of the D and G peaks was performed using Fityk 1.3.1 software. The textural properties of the samples were evaluated from N_2 adsorption isotherms measured at 77 K using a volumetric sorption analyser (Belsorp Mini-II, Microtrac Bel Ltd., Japan), and CO_2 adsorption isotherms measured at 273 K using a gravimetric sorption analyser (IGA-100, Hiden Isochema Ltd., UK).

2.3 CO_2 adsorption experiments and analyses

CO_2 sorption experiments were conducted at up to 2 MPa, and at various temperatures (273, 298 and 323 K) using a gravimetric sorption analyser (IGA-100, Hiden Isochema Ltd., UK) supplied with pure CO_2 gas (99.995 vol%, Linde Gas Ltd.) [7]. Measurements of CO_2 adsorption-desorption isotherms up to 100 kPa and 2 MPa were performed separately at different analyser settings. The CO_2 adsorption isotherms up to 100 kPa were performed twice to calculate the standard deviation. The CO_2 adsorption isotherms at pressures up to 2 MPa were conducted only once with highly accurate weight stability of ±0.0001 g. Prior to each sorption measurement, the target sample was evacuated overnight to 10^{-6} kPa at 423 K, using a fast response oven. Isotherms were collected whilst maintaining a pressure accuracy of ±0.02%. Each point on the isotherm required around 10 minutes to stabilisation and reach equilibrium.

The temperature was controlled using a water bath to an accuracy of ±0.05 K. Dynamic CO_2 adsorption was estimated via breakthrough experiments carried out at 298 K using the IGA-100 connected to a quadrupole mass spectrometer (HRP-20 QIC, Hiden Analytical Ltd.). Breakthrough curves were measured using a CO_2 to N_2 gas mixture of 15:85 vol% and a flow rate of 50 ml min^{-1}, according to a setup illustrated in our previous study [28]. Breakthrough curves were plotted displaying C/C_0 versus time (t), where C it the CO_2 concentration at time t and C_0 is the CO_2 concentration at $t = 0$, as determined by mass spectrometry.

The CO_2/N_2 selectivity ($S_{CO2/N2}$) was calculated using Ideal Adsorbed Solution Theory (IAST), based on pure-phase CO_2 and N_2 adsorption isotherms measured under the same experimental conditions [23]. Sips and Langmuir models were applied to fit the CO_2 and N_2 adsorption isotherms, respectively. The IAST CO_2 and N_2 adsorption isotherms for a respective CO_2/N_2 gas mixture were calculated using GraphIAST software [39].

Isosteric heats of CO_2 adsorption (ΔH_{st}) were calculated using the Clausius-Clapeyron equation, which describes the dependence of ΔH_{st} values on surface coverage (i.e. on the amount of CO_2 adsorbed) [40]. Isosteres were obtained at 273, 298 and 323 K, and the corresponding pressure values at fixed amount adsorbed were obtained from the Sips fitting results.

3. RESULTS AND DISCUSSION

3.1. Characterisation of carbon foam materials

3.1.1. Morphology

The morphology of the CF, C_3N_4/CF-1 and C_3N_4/CF-24 samples was investigated by SEM (Figure 1). At low magnification, the characteristic three-dimensional structure of carbon foams is evident as micron-scale spheroidal cells separated by thin cell walls [28]. The similarity of the three samples confirms that coating the CF scaffold with carbon nitride does not significantly affect the macrostructure. Higher magnification reveals more notable differences between the samples. Figure 1(c) shows that some regions of CF have a degree of nanoscale roughness, potentially indicating the presence of micropores. Figure 1(f) reveals a slightly different morphology for C_3N_4/CF-1, potentially depicting the deposited layer of carbon nitride particles [41,42]. Meanwhile, Figure 1(i), for C_3N_4/CF-24 larger particles with diameter of

several hundred nanometres are clearly observed to be adhered to the surface of the CF scaffold, also be assumed to be carbon nitride. As such the SEM results depict a clear progression between the uncoated CF sample, to the sample which underwent wet impregnation with DCD for only one hour (C_3N_4/CF-1), to the sample which was impregnated for 24 hours (C_3N_4/CF-24). The particle size distribution calculated from the low-magnification SEM images (Figure S1) using ImageJ software and presented in Figure S2 shows that most particles in all three samples were in the range of 10-60 μm, and the largest determined particles had size of about 280 μm.

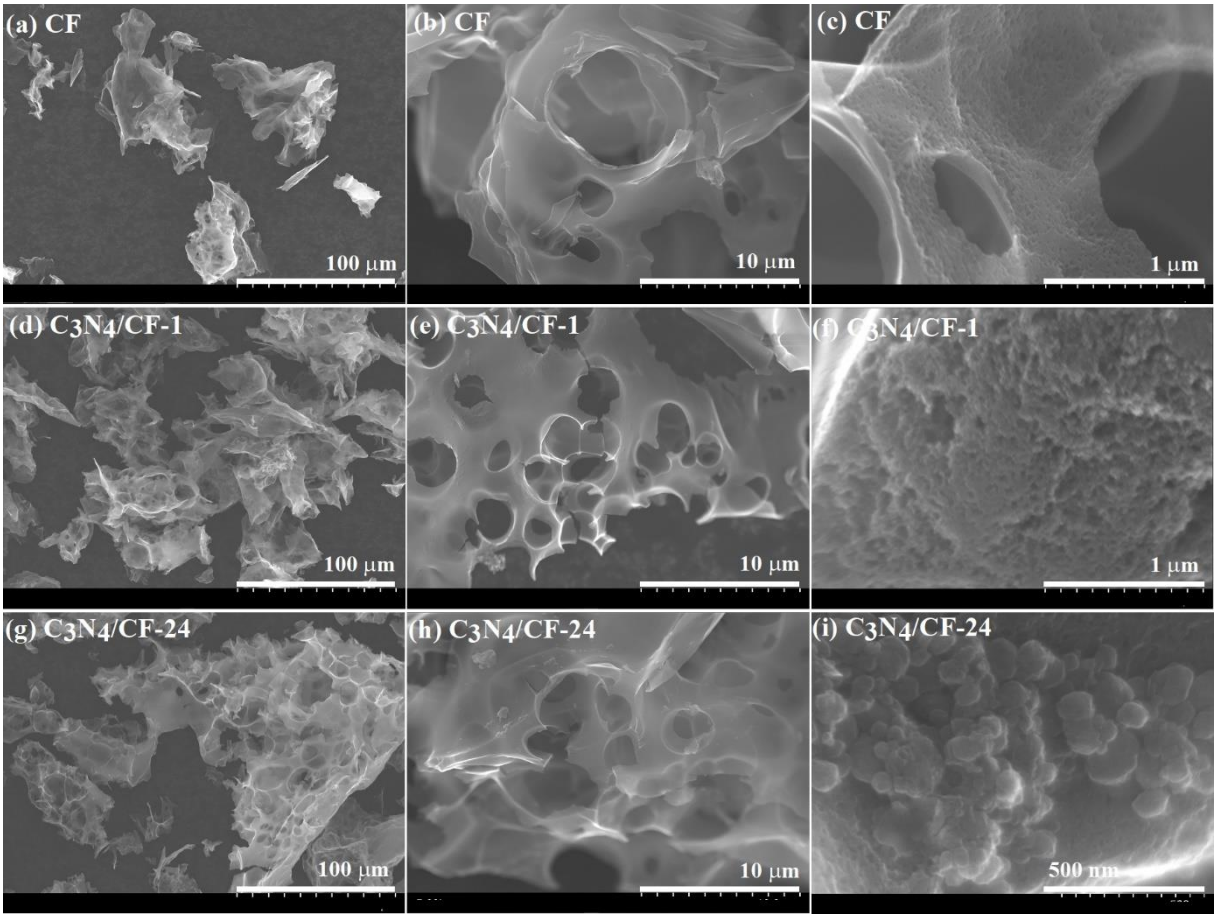

Figure 1. SEM images of the three adsorbents: (a-c) pure carbon foam (CF); (d-f) carbon foam coated with carbon nitride via wet impregnation for 1 hour (C_3N_4/CF-1); and (g-i) carbon foam coated with carbon nitride via wet impregnation for 24 hours (C_3N_4/CF-24).

3.1.2. Elemental composition

The bulk chemical composition of the three adsorbents was determined by CHNO elemental combustion analysis, revealing that the CF sample has only minimal nitrogen content

(0.3 at%), increasing to 5.3 at% for C_3N_4/CF-1 and to 17.0 at% for C_3N_4/CF-24 (Table S3). This confirms that (i) the DCD polymerisation step was successful, (ii) that coating CF with carbon nitride does indeed introduce significant amounts of nitrogen, and (iii) that the duration of the wet impregnation step has a major impact on the nitrogen content of the final product.

XPS was also performed to determine the abundance and the chemical state of nitrogen atoms in the samples. The survey spectrum contains characteristic peaks at binding energies of ~ 285 eV, 400 eV and 530 eV corresponding to C1s, N1s and O1s, respectively (Figure 2a). Here, the nitrogen content of CF is negligible, in agreement with the CHNO data. The nitrogen content increases to 6.2 at% for C_3N_4/CF-1, which again is close to the CHNO result, although slightly higher. Notably, for C_3N_4/CF-24, the nitrogen content according to XPS is just 5.3 at%, which is significantly lower than the value of 17.0 at% obtained via combustion analysis (Table S1). This discrepancy is attributed to bulk nature of combustion analysis compared with the quasi-surface sensitive nature of XPS, in which photoelectrons can only escape from a depth of several nm within the sample [43]. As such, these results indicate that a large proportion of nitrogen atoms in C_3N_4/CF-24 reside within the "bulk" material. An explanation for this is that DCD penetrates further into the micropores of CF during the longer wet impregnation stage, and carbon nitride is then embedded within those pores during the heat treatment step.

To gain further insight into the chemical environment of nitrogen atoms in the adsorbents, N1s spectra were recorded and deconvoluted into four peaks. These correspond to: sp^2-hybridized pyridinic nitrogen species (C=N-C, at 398.6 eV); tertiary nitrogen species or amines (C-$(N)_3$ or -NH_2, at 400.3 eV); hydrogenated pyridinic nitrogen species (C-NH-C, at ~401.5 eV); and oxidized nitrogen species (N-O, at 403.1 eV) (Figure 2b, Table S2). The ratio of different nitrogen contributions for both C_3N_4/CF-1 and C_3N_4/CF-24 are remarkably similar, with the highest abundance for pyridinic nitrogen, followed by tertiary / amine species and then hydrogenated pyridinic species and finally a small proportion of oxides. These proportions are quite typical of carbon nitride if the tri-s-triazine-type structure is considered. Deconvolution of C1s and O1s spectra was also performed (Figure S3, Table S3 and Table S4) [44–47].

Overall, the elemental analysis indicates that carbon nitride is successfully coated onto the surface of carbon foams using this method. As outlined in the introduction, this is expected to be beneficial for CO_2 adsorption via the introduction of Lewis base sites. However, it is also hinted that the micropores could be filled with carbon nitride, which may be detrimental to adsorption.

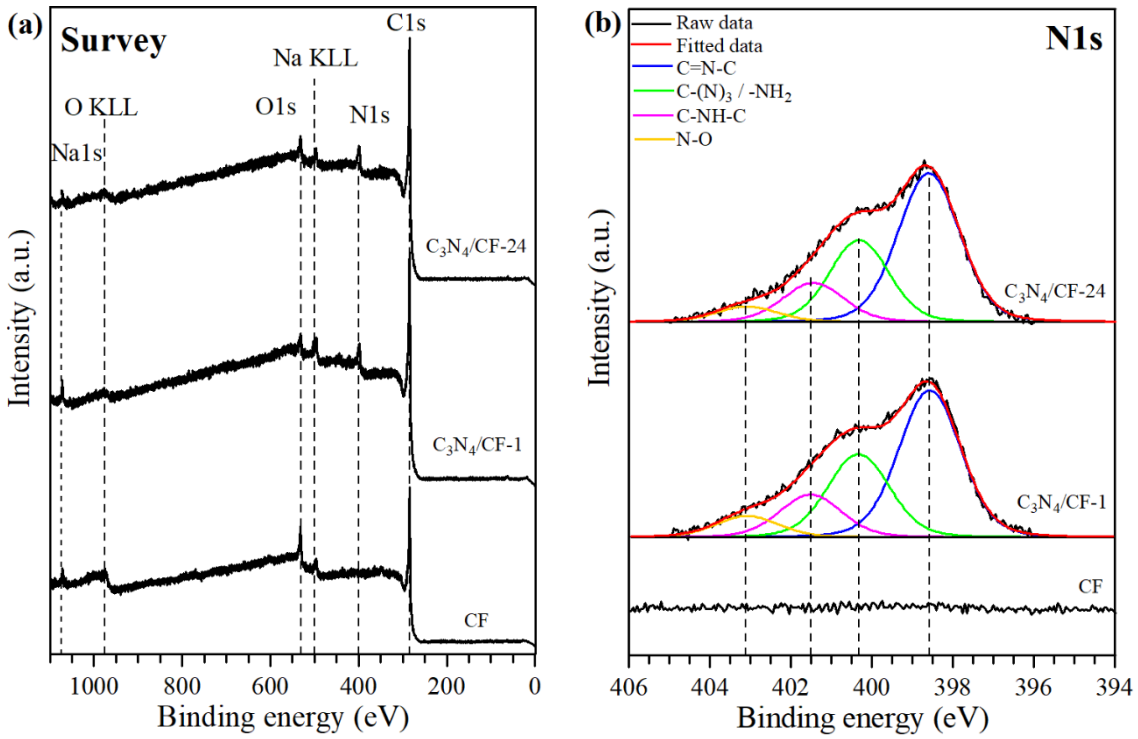

Figure 2. XPS spectra of the adsorbents: (a) survey spectrum; (b) N1s region.

3.1.3. Crystalline structure

The crystallinity of the adsorbents was assessed via XRD (Figure 3a). The XRD spectra all display a broad 2θ peak in the range of 15-30°, with a maximum at ~22°. This corresponds to the (002) plane of graphitic carbon with an interlayer distance of 0.4 nm indicating a relatively amorphous structure (i.e. significantly larger than the 0.36 nm of highly oriented pyrolytic graphite) [28]. Notably, a prominent shoulder is observed at 27.4° in the C_3N_4/CF-24 sample with a high nitrogen content of 17 at%. In contrast, this shoulder is absent in the C3N4/CF-1 sample, which has a lower carbon nitride content with 5-6 at% of nitrogen only. This corresponds to the (002) plane of graphitic carbon nitride, with a lattice parameter of 0.167 nm and an interlayer distance between triazine sheets of 0.32 nm [30,48]. The prominence of this shoulder in C_3N_4/CF-24 confirms that longer wet impregnation time results in the formation of more carbon nitride, in agreement with SEM and elemental analysis. Additionally, a small peak at ~ 44° is attributed to the (100) plane of graphitic carbon [37]. Overall, the peaks are not particularly sharp, indicating that both the CF scaffold and the carbon nitride coating are relatively amorphous materials.

The degree of crystallinity was also assessed via Raman spectroscopy, by calculating the ratio of the intensities (I_D/I_G) and the peak areas (A_D/A_G) of the D and G bands at 1338 cm^{-1} and ~ 1580 cm^{-1}, respectively (Figure 3b, Table S5). The D peak is indicative of breathing vibrations of sp^2 aromatic rings in carbon materials, and the G peak represents stretching vibrations of these rings [49]. Both the I_D/I_G and A_D/A_G ratios increase significantly from CF to C_3N_4/CF-1 to C_3N_4/CF-24. This signifies greater degree of disorder in the carbon structure after coating with carbon nitride, attributed to the increased presence of triazine aromatic rings. The 2D peak is generally associated with in-plane vibrational modes of the sp^2-bonded carbon and nitrogen atoms in the two-dimensional lattice, and the intensity, shape, and position are sensitive to the degree of graphitization, the presence of defects, and the stacking arrangement of carbon and nitrogen layers in the material [50]. In both CF and C_3N_4/CF-1 the 2D peak is relatively featureless, but a more pronounced fine structure at 2680 cm^{-1} is observed for the C_3N_4/CF-24 sample. This may be indicative of higher crystallinity in that sample, suggesting that graphitic carbon nitride (g-C_3N_4) may have been synthesized in this case. An excitation wavelength of 534 nm was used, so the number of layers is estimated to be less than five [50]. The formation of this graphitic phase could be due to confinement in micropores during polymerisation.

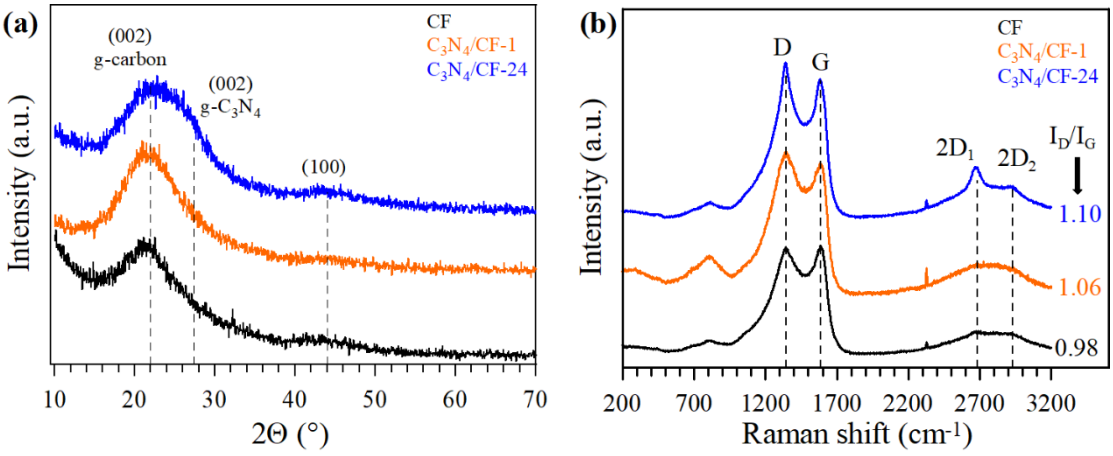

Figure 3. a) XRD patterns and b) Raman spectra of the three adsorbents.

3.1.4. Textural properties

Isotherms were measured in N_2 and CO_2 to assess the porosities and surface areas of the adsorbents. Micropores are defined as having a pore diameter below 2 nm, and sometimes a further distinction into supermicropores (ranging from 0.7 to 2 nm) and ultramicropores (below 0.7 nm) is made [51]. Meanwhile, mesopores are defined as having pore diameters between 2

and 50 nm. The N_2 adsorption isotherms measured at 77 K (Figure 4a) can all be classified as Type IV. A distinct knee at low relative pressures (P/P_s < 0.01, where P_s is the saturation pressure) indicates micropore filling, whilst the H4-type hysteresis loop at P/P_s > 0.4 is characteristic of capillary condensation in mesopores [23]. Similarly, in the case of CO_2 adsorption isotherms measured at 273 K (Figure 4b) micropore filling with CO_2 gas at P/P_s values of up to ~ 0.03 is also evident [52].

The ultramicropore volume was determined using the Dubinin-Radushkevich (DR) adsorption model applied to the CO_2 adsorption isotherms [53], while the micropore volume (V_{micro}) was obtained using the Lippens and de Boer V_{ads}-t plot models, applied to the N_2 adsorption isotherms [54]. All pore parameters determined from the adsorption isotherms are listed in Table 1. Meanwhile, the pore size distribution in the range 0.36 to 30 nm was obtained by applying the non-local density functional theory (NLDFT) adsorption model to the combined adsorption isotherms (Figure 4c, Figure S4a and Figure S4b). The results are in broad agreement with each other.

CF exhibits remarkable surface area (2537 m^2 g^{-1}), as well as the highest ultramicropore volume, micropore volume, and mesopore volume, translating into the largest total pore volume. Meanwhile, for C_3N_4/CF-1 there is a moderate decrease in the surface area and total pore volume, but only a slight decrease in ultramicropore volume. Finally, for C_3N_4/CF-24 there is a significant decrease in surface area, total pore volume, and ultramicropore volume. This further supports the hypothesis that wet impregnation for 24 h reduces porosity and surface area by blocking or filling micropores with carbon nitride.

Table 1. Specific surface area pore parameters obtained from combined NLDFT analysis of the CO_2 and N_2 adsorption isotherms measured at 273 K and 77 K, respectively.

Samples	S_{BET}[a]	V_{ultra}[b]	V_{micro}[c]	V_{meso}[e]	V_{tot}[d]	$d1$[f]	$d2$[f]	$d3$[f]	$d4$[f]
	$cm^3\ g^{-1}$	$cm^3\ g^{-1}$	$cm^3\ g^{-1}$	$cm^3\ g^{-1}$	$cm^3\ g^{-1}$	nm	nm	nm	nm
CF	2537	0.4617	1.3407	0.2664	1.6071	0.40	0.63	1.19	2.46
C_3N_4/CF-1	2127	0.4495	1.1011	0.1940	1.2951	0.41	0.60	1.21	2.46
C_3N_4/CF-24	1263	0.2774	0.6869	0.1116	0.7985	0.41	0.64	1.33	2.46

[a]*BET applied to the N_2 adsorption isotherm: specific surface area (S_{BET})*

[b]*DR applied to the CO_2 adsorption isotherms: ultramicropore volume (V_{ultra})*

[c]*Lippens and de Boer V_{ads}-t plot applied to the N_2 adsorption isotherm: micropore volume (V_{micro})*

[d]*Gurvitch applied to the N_2 adsorption isotherm: total pore volume (V_{tot}) at $p/p_s = 0.99$*

[e]*$V_{meso}=V_{tot} - V_{micro}$*

[f]*NLDFT applied to CO_2 and N_2 isotherms: ultramicropore (d1, d2), micropore (d3) and mesopore (d4) diameters*

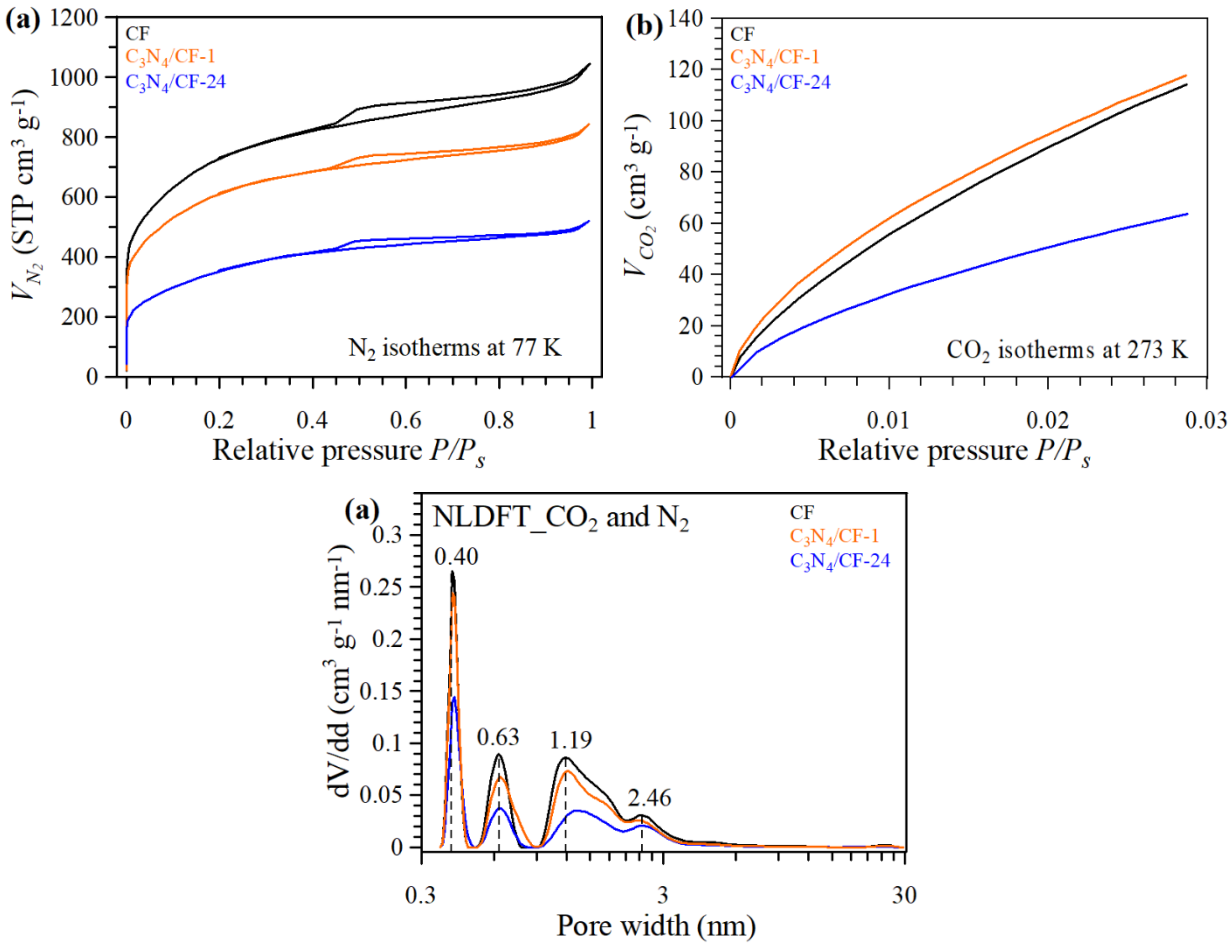

Figure 4. a) N_2 adsorption isotherms for the three adsorbents measured at 77 K. b) CO_2 adsorption isotherms measured at 273 K. c) Pore size distribution as determined by NLDFT.

3.2. CO_2 capture performance

3.2.1. Post-combustion capture

CO_2 adsorption-desorption isotherms for pressures up to 100 kPa at three temperatures are shown in Figure 5a-c, corresponding to post-combustion capture conditions. The amount of CO_2 adsorbed increases with pressure, and the highest CO_2 uptake occurs at the lowest temperature, as expected. The desorption isotherms closely follow the adsorption isotherms and are therefore not clearly visible in these graphs, but this indicates that adsorption is highly reversible. Numerical values for the CO_2 uptake (η_{CO2}) at different temperatures and their standard deviations, ranging up to ±0.05 are given in Table 2.

Under these conditions, C_3N_4/CF-1 exhibits the highest CO_2 uptake (i.e. 5.24 mmol g^{-1} at 273 K), followed by CF (5.09 mmol g^{-1}) and then C_3N_4/CF-24 (2.83 mmol g^{-1}). To help understand this trend, it should be noted that ultramicropores are known to enhance CO_2 adsorption, due to overlapping dipole moments of the CO_2 molecules and pore walls, leading to more efficient packing [55]. Furthermore, nitrogen functionalities can serve as Lewis base sites favourable for CO_2 adsorption via weak chemisorption [26]. Analysis of CO_2 adsorption mechanism, investigating adsorption energy of different nitrogen functionalities with molecules CO_2 (E_{ad}) showed that quaternary nitrogen (E_{ad} = -14.88 kJ mol^{-1}) and pyrrole nitrogen (E_{ad} = -17.47 kJ mol^{-1}) enhance the surface CO_2 adsorption, whereas pyridine nitrogen (E_{ad} = -22.57 kJ mol^{-1}) enhances the edge CO_2 adsorption [36]. In this study, the XPS results confirmed that carbon nitride was the major nitrogen coating the carbon foam surface, which is composed of pyridinic nitrogen, followed by tertiary/amine species, then hydrogenated pyridinic species and small amount of oxidized nitrogen (Figure 2, Table S2). Therefore, the trend of CO_2 uptake shown in Figure 5 is attributed to the fact that (i) C_3N_4/CF-1 combines large ultramicropore volume with an abundance of nitrogen sites, whilst (ii) CF only has large ultramicropore volume (and no nitrogen sites), and (iii) that C_3N_4/CF-24 has dramatically reduced pore volume despite its high nitrogen content. This underscores the significance of nitrogen functionality in combination with the presence of micropores for post-combustion capture.

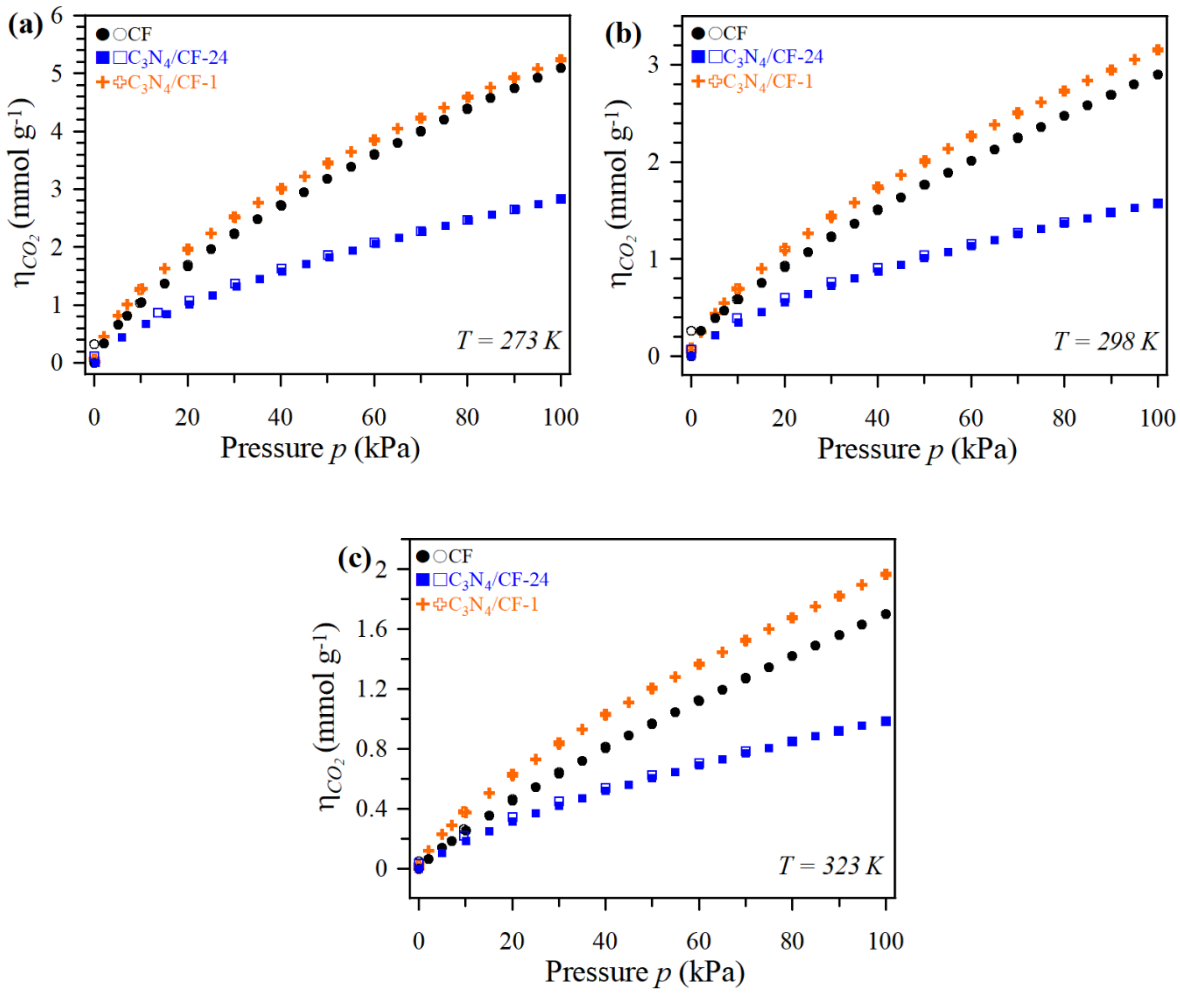

Figure 5. CO_2 adsorption isotherms measured at 100 kPa and at: a) 273 K, b) 298 K, and c) 323 K. Bold symbols correspond to adsorption isotherms and empty symbols correspond to desorption isotherms. Desorption isotherms are not clearly visible as they closely follow the adsorption isotherms.

Table 2. CO_2 uptake of the carbon foam samples at temperatures of 273, 298 and 323 K, and at pressures of 100 kPa and 2 MPa.

Sample	η_{CO2} at 273 K (mmol g^{-1})		η_{CO2} at 298 K (mmol g^{-1})		η_{CO2} at 323 K (mmol g^{-1})	
	100 kPa	2.0 MPa	100 kPa	2.0 MPa	100 kPa	2.0 MPa
CF	5.09±0.03	25.52	2.90±0.04	18.44	1.70±0.04	14.09
C_3N_4/CF-1	5.24±0.05	21.84	3.16±0.01	15.70	1.97±0.02	12.04
C_3N_4/CF-24	2.83±0.03	11.92	1.57±0.04	8.19	0.99±0.02	6.40

3.2.2. Pre-combustion capture

Meanwhile, CO_2 adsorption-desorption isotherms for pressures up to 2 MPa are shown in Figure 6a-c, corresponding to pre-combustion capture conditions [56]. Notably, in contrast with the lower pressure measurements, CF now exhibits the highest CO_2 uptake, adsorbing up to a maximum of 25.52 mmol g^{-1} at 273 K (see Table 2). This is comparable with the highest reported uptake values in the literature under similar conditions. Meanwhile, C_3N_4/CF-1 has slightly lower uptake (21.84 mmol g^{-1}), and C_3N_4/CF-24 has significantly lower CO_2 uptake (11.92 mmol g^{-1} g).

In this case (i.e. higher pressure), the trend can be attributed to an increased presence of supermicropores (0.7 to 2.0 nm) and small mesopores (2.0 to 3.0 nm) in CF (Figure 4c), which tend to become filled at higher pressures, and do not take part in adsorption at lower pressures [68]. Indeed, it is known that pores up to 10 nm are completely filled with CO_2 at pressures up to the vapour saturation pressure of CO_2, and pores smaller than 3 nm should be filled at pressures up to $P/P_s \sim 0.58$ (i.e. 2.0 MPa at 273 K) [57]. Figure S5 shows the CO_2 adsorption capacity at 2 MPa and 273 K, depending on different parameters, including nitrogen content (Figure S5a), S_{BET} (Figure S5b), V_{ultra} (Figure S5c), V_{micro} (Figure S5d), V_{meso} (Figure S5e) and V_{tot} (Figure S5f). All trends, except for V_{ultra} ($R^2 = 0.8994$) and V_{meso} ($R^2 = 0.9270$), show good linear fits with correlation coefficients higher than 0.9800. The best fit for CO_2 uptake was found with nitrogen content ($R^2 = 0.9991$). However, since nitrogen content is directly related to S_{BET} (Figure S5g), it can be concluded that CO_2 uptakes are primarily determined by the specific surface area, which is influenced by the volume of micropores and mesopores (i.e. total pore volume V_{tot}). Thus, CF, with the highest S_{BET} value and V_{tot} (Table 1), showed the highest CO_2 uptake at 2 MPa. Conversely, the C_3N_4/CF-24, with the lowest S_{BET} value and V_{tot} among the studied materials, adsorbed the least CO_2 under the same pressure and temperature conditions. This conclusion aligns well with previous studies [58,59]. Another explanation of CO_2 adsorption can be that in the case of adsorbents with larger adsorption energy (due to the introduction of Lewis base sites), the increase in CO_2 uptake ($d\eta/dP$) at low partial pressure is relatively fast compared to materials with lower adsorption energy, the result being that saturation can occur at lower partial pressure. Thus C_3N_4/CF-1 may display higher uptake than CF at 100 kPa due to the presence of nitrogen, but lower uptake at 2 MPa due to lower total adsorption capacity. This implies that for CO_2 uptake at higher pressures (relevant to pre-combustion capture), nitrogen-doping has minimal influence on adsorption capacity, with porosity being the dominant factor.

Meanwhile, the Sips adsorption model was used to determine the homogeneity of the sample surfaces [60], with Sips fits in excellent agreement with the corresponding adsorption isotherms (Figure 6a-c, Figure S6). Analysis of the fitting data (Table S6) reveals Freundlich exponent values of n <1, indicating heterogeneous adsorption. Notably, C_3N_4/CF-1 and C_3N_4/CF-24 have a greater degree of heterogeneity than CF. This is as expected since two different materials (carbon foam and carbon nitride) are present in the same adsorbent which have presumably distinct adsorption properties.

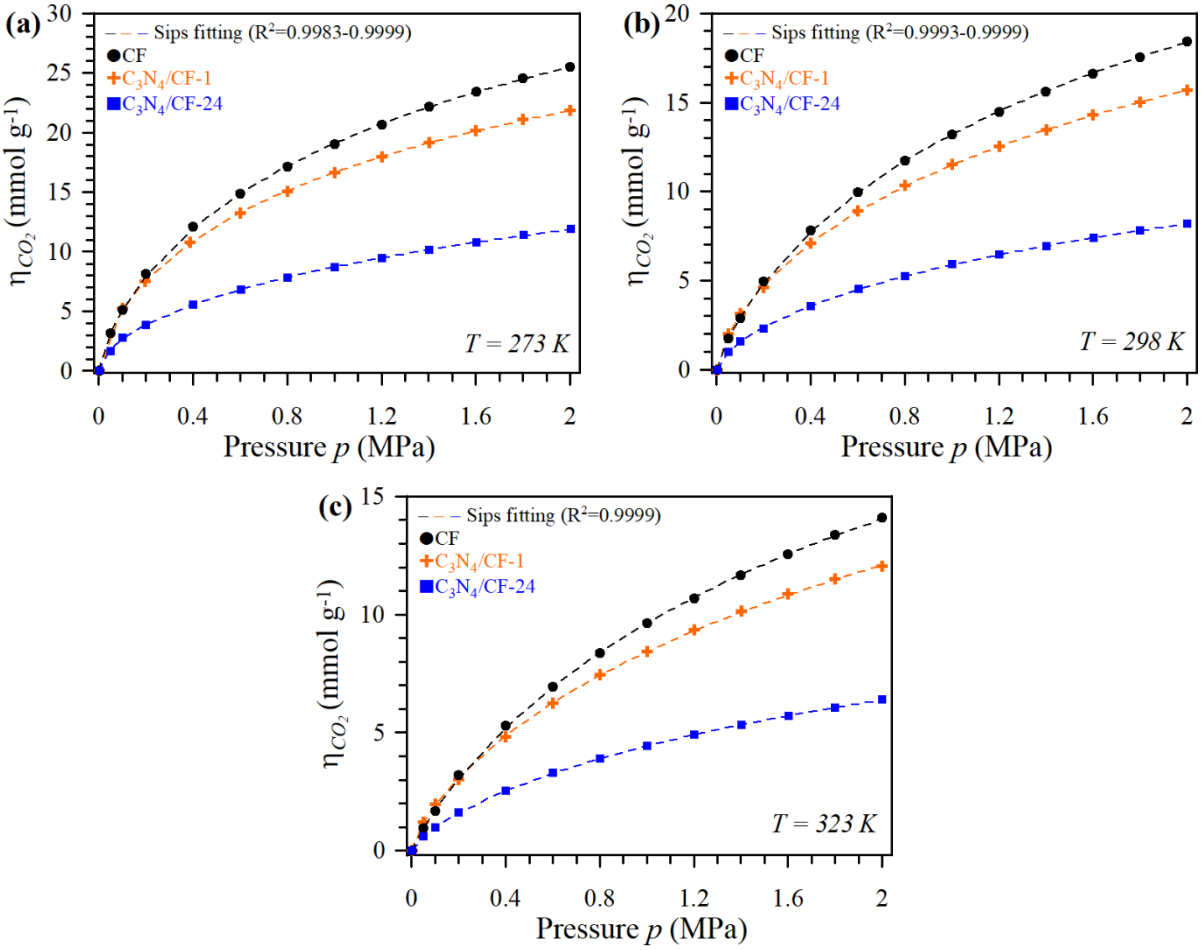

Figure 6. CO_2 adsorption isotherms measured at 2 MPa and at: a) 273 K, b) 298 K and c) 323 K. Dotted lines correspond to the Sips fittings.

3.2.3. Comparison with literature

To add context to the CO_2 adsorption capacities of carbon foam samples, the properties are herein compared with data reported for similar materials and conditions in the literature (Table

3). Differences in experimental conditions, such as temperature and pressure, as well as variations in the porous and chemical structure of the carbon materials, significantly impact reported CO_2 sorption capacities. As discussed above, adsorption capacity increases with higher pressure and lower temperature. Additionally, the specific surface area, porosity and surface chemistry of the carbon materials also play critical roles. Based on this, the uptake values and CO_2/N_2 selectivity of the carbon foam materials presented here are comparable to reported values of the best carbon materials in the comparable study in the literature (Max. η_{CO2}). Specifically, different pore parameters (S_{BET}, V_{micro}, V_{meso}, V_{tot}) and the presence or absence of nitrogen content under similar pressure (100 kPa and 2 MPa) and temperature (273 K and 298 K) are focused on. In this comparison, differences are accounted for by normalising the CO_2 uptake to the pressure and temperature conditions applied in this work. This approach allows for a clearer assessment of the performance of the CF and C_3N_4-coated carbon foam samples.

Overall, nitrogen-doped carbons in Table 3 have predominantly been measured at low atmospheric pressures due to their higher selectivity in that region (as discussed in the next section) [25,31,35,40,61–63]. Especially, polyethyleneimine-functionalized carbon nitride exhibited extremely high CO_2/N_2 selectivity (> 6500) due to strong reactivity of amine groups with CO_2 [35]. In contrast, pure carbon materials tend to be measured at higher pressure, where porosity dominate over adsorption energy [6–8,64–67]. Some carbon materials exhibited high adsorption capacity due to their high specific surface areas in addition to the presence of Lewis base centres that attract CO_2 [28,58,68–74]. In particular, amine-functionalized porous carbon [74] exhibited exceptionally high CO_2 uptake of ~25.94 mmol g^{-1} at 2 MPa and 298 K, preferably attributed to high microporosity. Other porous carbons [17,32–34,59,75] displayed varying CO_2 uptake based on their micropore and total pore volumes.

Table 3. Comparison of the CO_2 adsorption capacities for various porous carbon in the literature, with the carbon foam materials presented in this study.

Sample	S_{BET} (m^2 g^{-1})	V_{micro} (cm^3 g^{-1})	V_{meso} (cm^3 g^{-1})	V_{tot} (cm^3 g^{-1})	N content	T (K)	P (MPa)	Max. η_{CO2} (mmol g^{-1})	IAST $S_{CO2/N2}$ (CO_2:N_2)	Study
Carbon foam (CF)	2537	0.46	0.27	1.61	-	273	0.1	5.1	-	This study
						273	2.0	25.5	-	
						298	0.1	2.9	14 (15/85)	
						298	2.0	18.4	-	
Carbon nitride-coated carbon foam	2127	0.45	0.19	1.30	5.3 at%	273	0.1	5.2	-	This study
						273	2.0	21.8	-	
						298	0.1	3.2	21 (15/85)	
						298	2.0	15.7	-	
Activated carbon	3575	1.22	0.61	1.83	-	298	0.1	~ 2.5	-	[6]

						298	2.0	~ 19.0	-	
Activated mesoporous carbon	1462	0.27	3.94	4.20	-	273 298	0.1 2.0	3.2 11.3	55 (15/85) -	[8]
Activated microporous carbon	3537	-	-	1.85	-	298 298	0.1 2.0	2.8 21.1	- -	[65]
Activated carbon	-	-	-	-	-	273	2.0	~ 10.5	-	[66]
Activated carbon	-	0.65	0.03	-	-	273	2.0	~ 14.0	-	[67]
Ordered mesoporous carbon	1343	0.17	3.42	-	-	298 298	0.1 2.0	1.5 9.2	- -	[7]
Ordered mesoporous carbon	1491	-	-	1.30	-	298	2.0	~ 10.2	-	[64]
Ordered mesoporous carbon	1396	0.14	1.12	-	-	298	0.1	~ 2.2	-	[17]
Carbon nitride aerogel	~400	-	-	-	8 wt%	300	0.1	4.2	113 (10/90)	[31]
Microporous carbon nitride	130	-	-	0.40	66 wt%	273	2.0	~ 3.7	-	[32]
Ordered mesoporous carbon nitrides	232	-	-	0.28	61 at%	273	0.1 2.0	~ 0.6 ~ 3.2	-	[33]
Mesoporous carbon nitride	901	-	-	1.02	C/N=2.9	273	0.1 2.0	~ 2.5 ~ 7.0	- -	[34]
Polyethylenimine-functionalized carbon nitride	1.2	0	-	0	41.9 wt%	273	0.1	1.8	6588 (15/85)	[35]
Nitrogen-doped porous carbon	1209	0.34	0.07	-	6.1 at%	298	0.1	4.2	56 (15/85)	[25]
Nitrogen-doped carbon foam	1549	0.60	0.20	0.81	7.3 wt%	273 298	0.1 0.1	5.1 3.2	- ~ 20 (15/85)	[28]
Nitrogen-doped carbon cryogel	2084	0.74	1.24	-	3.9 at%	273 298	0.1 0.1	6.4 3.9	115 (15/85) 90 (15/85)	[40]
Nitrogen-containing activated carbon	2403	0.30	1.00	1.30	3.0 wt%	273	0.1 2.0	5.2 25.1	11 (15/85) -	[58]
Nitrogen-doped carbon nanofiber	1878	0.41	-	-	6.6 wt%	273 298	0.1 0.1	6.8 -	32 (15/85) 40 (15/85)	[61]
Nitrogen-doped mesoporous carbon	354	-	-	0.24	6.2 wt%	273 298	0.1 0.1	1.9 1.7	65 (15/85) 79 (15/85)	[62]
Nitrogen-doped graphene-like meso-macroporous carbons	404	0.02	1.1	1.12	22.3 wt%	273 298	0.1 0.1	3.4 2.7	62 (15/85) 92 (15/85)	[63]
Nitrogen-doped microporous carbon	2067	0.83	-	0.71	0.6 wt%	273 298	0.1 0.1	6.6 4.3	20 (15/85)	[68]
Nitrogen-doped activated carbon	1495	0.66	-	0.73	3.8 %	273	0.1	7.9	17 (15/85)	[69]
Nitrogen-doped activated carbon	1496	0.45	-	0.79	8.6 %	273 298	0.1 0.1	5.8 -	- 15 (15/85)	[70]
Nitrogen-doped porous carbon	2340	1.16	-	1.35	2.5 wt%	273 298	0.1 0.1	5.4 2.9	- ~ 20 (10/90)	[71]
Nitrogen-rich mesoporous spheres	860	-	-	0.46	-	298	0.1	4.9	-	[72]
Nitrogen-doped nanoporous carbon	1335	-	-	0.78	2.6 at%	273 298	0.1 0.1	6.0 3.5	- -	[73]

Amine-functionalized porous carbon	3492	-	-	1.33	-	298 298	0.1 2.0	- 25.9	~ 60 (15/85) -	[74]
N-rich activated carbon	633	0.64	-	0.73	9.4 at%	298	0.1 2.0	2.17 ~ 5.5	- -	[75]
Nitrogen, Sulfur-doped porous carbon	973	0.25	0.25	0.50	4.1 wt%	273	0.1 2.0	3.1 7.9	33 (15/85) -	[59]

3.2.4. Ideal Adsorbed Solution Theory and CO_2/N_2 Selectivity

The selectivity towards either CO_2 or N_2 adsorption ($S_{CO2/N2}$) is a crucial factor in designing industrial adsorption processes. Here, a practical scenario is simulated using the Ideal Adsorbed Solution Theory (IAST), with a post-combustion flue gas composition of 15 vol% CO_2 and 85 vol% N_2 at 298 K [23]. The high degree of accuracy of the measurements is confirmed by the excellent fits obtained for both pure CO_2 and N_2 adsorption isotherms, using the Sips adsorption model for CO_2 [76] and the Langmuir model for N_2 [37] (Figure 7a).

The values for selectivity obtained at 5 kPa are: 17.3 for CF, 15.6 for C_3N_4/CF-24, and 20.0 for C_3N_4/CF-1 (Figure 7b). This trend clearly aligns with the nitrogen content and amount of ultramicropores of the samples: C_3N_4/CF-1 exhibits high V_{ultra} (0.45 $cm^3\ g^{-1}$) and high nitrogen content (5.3 at%), thus demonstrating the highest selectivity, while CF has with high V_{ultra} (0.46 $cm^3\ g^{-1}$) but negligible nitrogen content has middle selectivity, and C_3N_4/CF-24 with the highest nitrogen content (17.0 at%) and the lowest V_{ultra} (0.28 $cm^3\ g^{-1}$) results in the lowest selectivity. This trend indicates strong binding between CO_2 molecules and nitrogen functionalities, in addition to CO_2 physically adsorbing in ultramicropores through van der Waals forces. Meanwhile, the selectivity decreases with increasing pressure for CF, which is attributed to competitive adsorption: at higher pressure, more molecules of all components become more available for adsorption on a limited number of ultramicropore sites, regardless of selectivity. Conversely, the selectivity slightly increases for C_3N_4-coated carbon foams with pressure increase, showing a more intense increase at the beginning of the sorption process. This phenomenon can be explained by CO_2 having a preference over N_2 for adsorption by nitrogen functionalities due to the more vital binding interaction (E_{ad} > -15 kJ mol^{-1}) compared to the weaker interaction with N_2 (E_{ad} < -13 kJ mol^{-1}) [36,77]. At 100 kPa selectivities of 13.9, 18.4 and 21.2 are obtained for CF, C_3N_4/CF-24 and C_3N_4/CF-1, respectively. Overall, these values are competitive with published results for porous carbons measured under similar conditions

[68,70,71] (Table 3), highlighting the potential of carbon nitride-coated carbon foams to be applied in industrial gas separation processes.

Following the principles of IAST, the CO_2 and N_2 adsorption isotherms were calculated for a gas mixture comprising 15 vol% CO_2 and 85 vol% N_2, using GraphIAST software [39] (Figure 7c). Notably, C_3N_4/CF-1 exhibits high CO_2 uptake of 0.81 mmol g^{-1}, surpassing that of CF (0.72 mmol g^{-1}). In contrast, C_3N_4/CF-24 displays the lowest uptake (0.41 mmol g^{-1}). This pronounced disparity underlines the critical importance of selecting an optimal amount of carbon nitride relative to the porous carbon foam to achieve the highest selectivity. The properties must be finely balanced, considering not only the carbon nitride content, but also the micropore volume since both factors significantly influence the overall adsorption performance and selectivity.

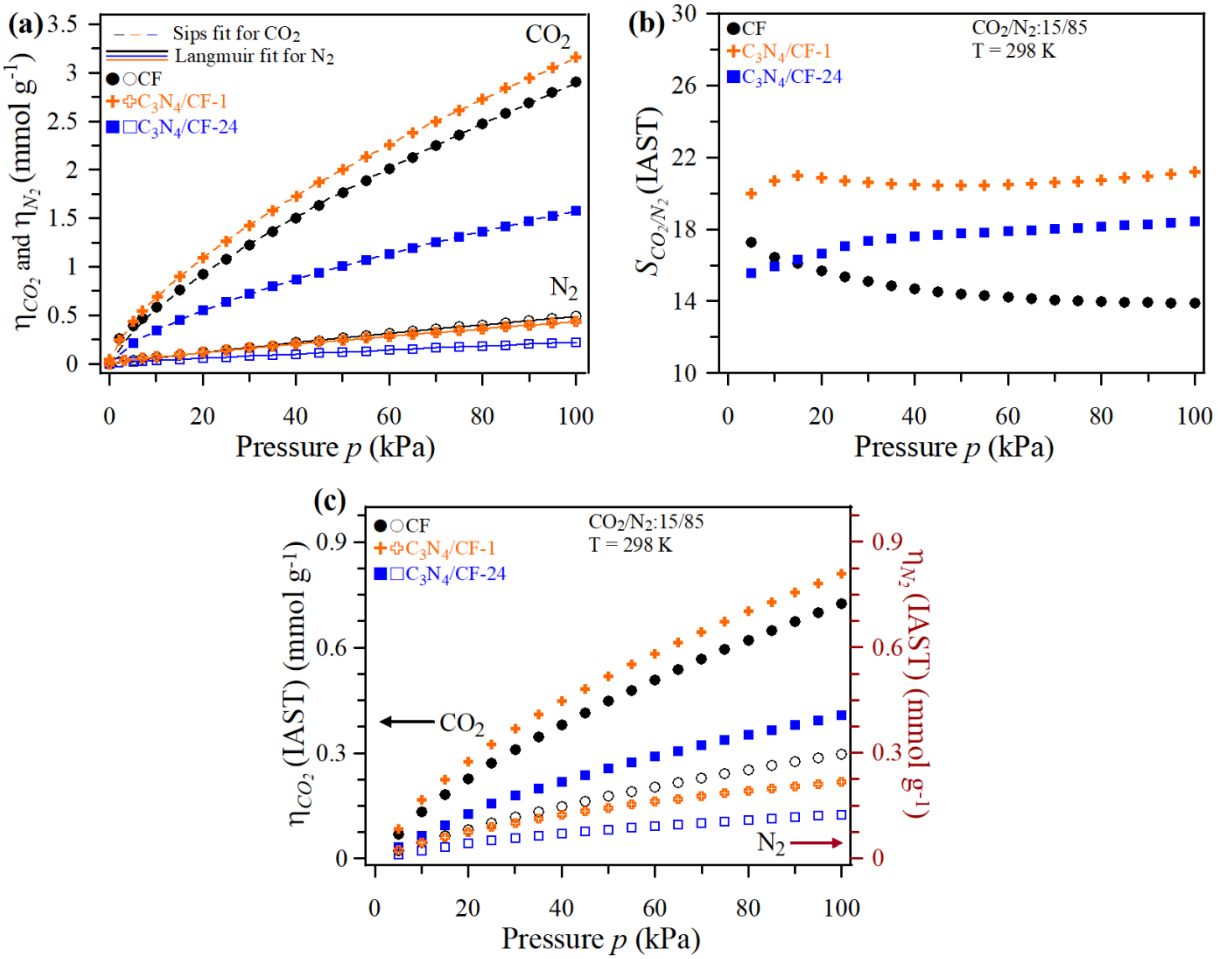

Figure 7. CO_2/N_2 selectivity: a) Experimental CO_2 and N_2 adsorption isotherms fitted with the Sips and Langmuir models; b) CO_2/N_2 selectivity; and c) CO_2 and N_2 adsorption isotherms calculated for the 15 vol% CO_2 - 85 vol% N_2 gas mixture using IAST. Bold symbols represent

CO_2 adsorption isotherms, empty symbols represent N_2 adsorption isotherms, dotted lines display Sips fitting and solid lines represent Langmuir fitting.

3.2.5. Breakthrough experiments

Experimental dynamic breakthrough curves were obtained at 298 K and 100 kPa (Figure 8a-c), using a 15 vol% CO_2 - 85 vol% N_2 gas mixture to simulate post-combustion flue gas. The resulting dynamic CO_2 uptake values were 0.35, 0.54 and 0.44 mmol g^{-1} for CF, C_3N_4/CF-1 and C_3N_4/CF-24, respectively. Both nitrogen-containing samples exhibited better performance than pure CF, as expected in this pressure regime, as outlined above. The best-performing sample was C_3N_4/CF-1, attributed to the combination of suitable porosity and high nitrogen content. This trend is consistent with the calculations obtained via IAST, however the experimental adsorption values are slightly lower (see Figure 7c). This may be attributed to the small sample size used here, resulting in a relatively short length of the packed bed, and thus there may be insufficient time to reach equilibrium before breakthrough is observed in this case. The values are compared with the literature in Table 4.

Meanwhile, the breakthrough time (t_b) recorded at C/C_o = 0.05 was ~1.25 mins for all three samples. These breakthrough times are rather short, but this is again attributed to the relatively small sample size used in this case (several tens of milligrams), which was unavoidable due sample synthesis scale limitations. In other studies reporting longer breakthrough times, gram-scale samples were used [78–80]. Recalculating an equivalent breakthrough time for a hypothetical packed bed with 1 g of the three carbon foam adsorbents results in values ranging from 45.4 to 75.3 min, which are comparable to values reported in the literature [81,82]. Repeating these results with gram-scale samples will be imperative for verification of these breakthrough results, so scale-up of carbon foam synthesis will be the subject of future studies.

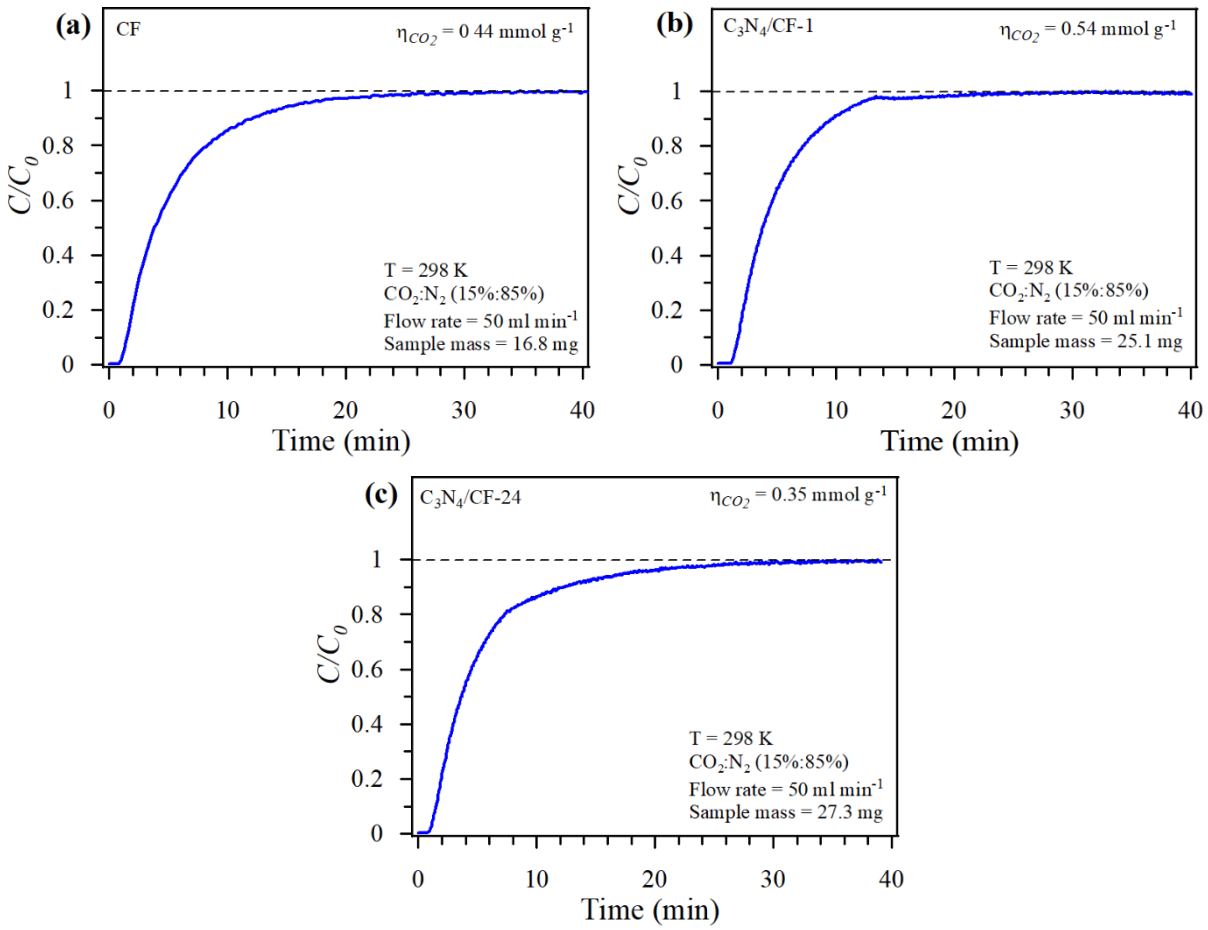

Figure 8. Breakthrough curves for a 15 CO_2 vol% - 85 vol% N_2 gas mixture for: a) CF, b) C_3N_4/CF-1 and c) C_3N_4/CF-24.

Table 4. Comparison of dynamic CO_2 uptake of the carbon foam materials with literature data.

Sample	S_{BET} (m^2 g^{-1})	Temperature (K)	Gas mixture (CO_2/N_2 vol%)	Flow rate (ml min^{-1})	CO_2 uptake (mmol g^{-1})	Breakthrough time (min g^{-1})	Study
Carbon foam	2537	298	15/85	50	0.44	75.3	This study
Carbon nitride-coated carbon foam	2127	298	15/85	50	0.54	49	This study
Activated 3D-ordered micromesoporous carbon	1462	298	15/85	50	0.29	49.1	[8]
Activated carbon	1922	303	20/80 20/80	50 70	1.31 1.20	3.2 2.2	[78]
Nitrogen-doped carbon foam	1064	298	15/85	50	0.84	20.2	[28]
Nitrogen-doped activated carbon	1495	298	15/85	50	0.99	10.6	[69]

Nitrogen-doped mesoporous carbons	266	303	5/95 7.5/92.5 10/90 12.5/87.5%	80	0.43 0.59 0.78 0.83	1.9 < 1.9 < 1.9 < 1.9	[79]
Nitrogen-doped porous carbon	1068	298	15/85	20	-	40	[81]
Nitrogen-containing carbon	606	313	15/85	2	1.11	40	[82]
Nitrogen-doped porous carbon	2779	298	10/90	-	~ 1.6	13.4	[83]

3.2.6. Isosteric heats of adsorption

The isosteric heats of CO_2 adsorption (ΔH_{st}) were determined from adsorption isotherms recorded at 273 K, 298 K, and 323 K and at pressures up to 2 MPa, employing Clausius-Clapeyron theory [84]. The isosteric heats serve as vital indicators of strength of interaction between CO_2 molecules and the adsorbent surface. In general, ΔH_{st} values below ~40 kJ mol^{-1} signify physisorption, whereas values above ~80 kJ mol^{-1} indicate chemisorption [85]. Lower isosteric heats are generally more favorable for adsorbent regeneration.

Isosteric heats can be calculated by plotting plotting *ln(p)* versus *1/T* at fixed adsorbed amount (i.e. under isosteric conditions). Here, this was performed from 0.5 to 14 mmol g^{-1} (Figure S7), resulting in isosteric heats ranging from 19 to 30 kJ mol^{-1}, indicating physical adsorption (Figure 9). In all three samples, ΔH_{st} increases substantially at lower values of CO_2 adsorption (η), which has also been reported elsewhere [84,86,87]. One explanation for this is that at lower values of η, adsorbate molecules are more likely to interact with the most energetically favorable sites on the adsorbent surface, leading to stronger binding. As more adsorbate molecules occupy the surface, the adsorbate binds to the remaining less favorable sites, leading to weaker binding (i.e. lower isosteric heat of adsorption). An alternative explanation is that this is simply an artifact of the limitations of the Sips model as η approaches zero (i.e. the Sips model does not simplify to Henry's law in the limit of low partial pressure [28]). To account for this, the following interpretations focus on the isosteric heat at moderate values of η (i.e. 6 mmol g^{-1}).

Comparing the three samples, pure CF has relatively low isosteric heat (~19.5 kJ mol^{-1}). Meanwhile, C_3N_4/CF-1 has significantly increased isosteric heat (~21.5 kJ mol^{-1}). However, there is then a significant drop in the isosteric heat for C_3N_4/CF-24, to a value similar to that of pure CF (~19.5 kJ mol^{-1}). An explanation for this involves the combined effects of enhanced

gas-surface interactions within micropores and increased surface interactions due to the introduction of Lewis base sites. Pure CF has a certain isosteric heat due to the presence of micropores, into which CO_2 molecules can enter and experience stronger binding by interacting with multiple surfaces simultaneously. Adding a small amount of carbon nitride (as in C_3N_4/CF-1) retains access to these micropores, but also introduces Lewis base sites further increasing the interaction strength with CO_2. Further increasing the amount of carbon nitride decreases the isosteric heat despite the larger nitrogen content. This is attributed to the blocking of micropores, thus preventing enhanced gas-surface interactions with CO_2 in the micropores. The isosteric heats of the studied carbon foam samples are comparable with reported values for other porous carbons [25,61,88], but lower than some reports for nitrogen-doped carbons [74,82].

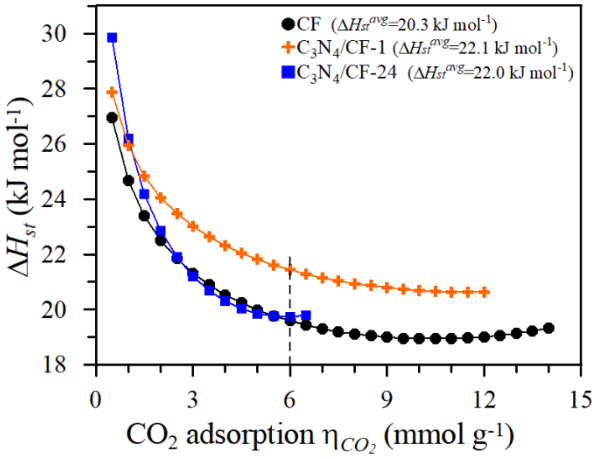

Figure 9. Isosteric heats of CO_2 adsorption as function of adsorption capacity.

3.2.7. Regenerative capability of the adsorbents

Finally, the regenerative performances of CF and C_3N_4/CF-1 were evaluated over 15 adsorption-desorption cycles conducted at 298 K and 100 kPa (Figure 10). Overall, the samples displayed remarkable stability, but there are subtle differences between the compared samples. For pure CF a slight decrease in the maximum amount adsorbed is observed after the first cycle (Figure 10a), which could be attributed to pore blocking, e.g. by residual CO_2 in ultramicropores. In contrast, the maximum amount adsorbed for C_3N_4/CF-1 remains constant, but the residual amount adsorbed increases slightly over the first six cycles (Figure 10b), which could be attributed to strong binding between CO_2 molecules and nitrogen groups on the carbon surface. These findings highlight the interplay between pore structure and surface chemistry on the regenerative behaviour of adsorbent. However, these minor changes in adsorption are small

compared to the total amount adsorbed and are not expected to significantly affect industrial application of these materials. When comparing the regenerative ability of CF and C_3N_4/CF-1 with commercial activated carbon [89], both materials show robust regeneration capabilities. However, carbon foam and carbon nitride-coated carbon foams offer distinct advantages due to their higher specific surface area and the presence of Lewis base sites. These attributes enhance CO_2 uptake and CO_2/N_2 selectivity compared to commercial activated carbons.

On the other hand, it should be noted that scaling up the synthesis of both pure carbon foams and carbon nitride-coated carbon foams presents significant challenges for industrial applications. These include (i) optimization of the synthesis parameters, i.e. temperature, heating rate, time, precursor concentration, inert atmosphere etc. to maintain the carbon foam properties observed at the laboratory scale, (ii) achieving uniform coating of carbon foam with carbon nitride to increase a large active surface for CO_2, (iii) handling of hazardous chemicals and safety issues, (iv) quality control measurements to ensure the reproducibility of the carbon foam properties, and (v) managing the material coasts. Solutions for these challenges include performing systematic studies to determine the optimal conditions for large-scale synthesis and using pilot-scale reactors to refine these parameters before full-scale production, ensuring consistency and reproducibility; using chemical vapor deposition (CVD) or atomic layer deposition (ALD) methods to achieve uniform coating with carbon nitride; implementing safety training programs and enforcing to strict operational guidelines to minimize risks associated with hazardous chemicals used in the synthesis process; verifying and maintaining the desired porous and mechanical properties using reliable quality control measures; and optimizing resource utilization, and developing recycling strategies for by-products to reduce overall production expenses.

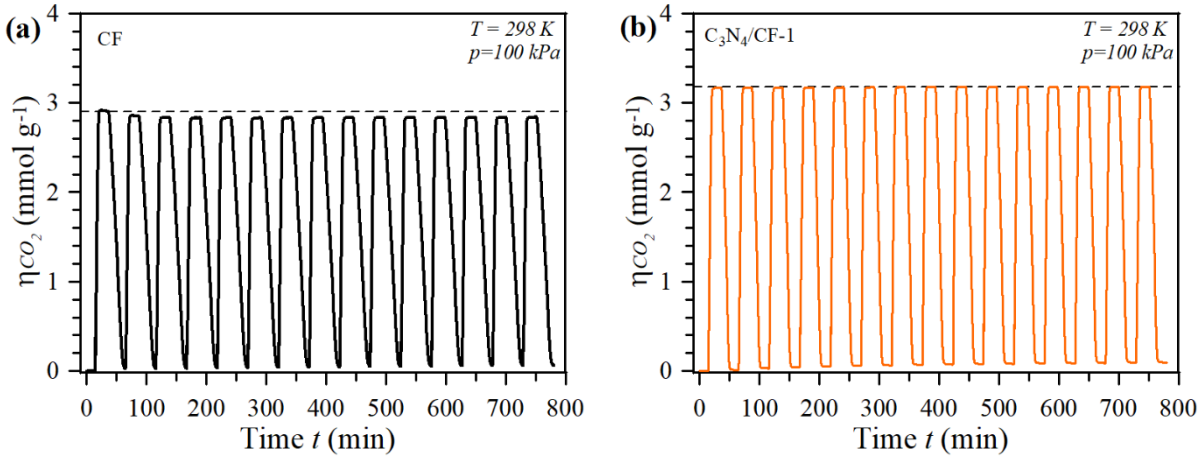

Figure 10. CO_2 adsorption-desorption cycling at 298 K and a pressure range of 0-100 kPa for a) CF, and b) C_3N_4/CF-1 adsorbents.

4. Conclusions

In this comprehensive study, hierarchically porous nitrogen-doped carbon foam adsorbents were synthesized and characterised. Carbon foam (CF) was obtained via thermal decomposition of sodium ethoxide, exhibiting exceptional surface area (2537 m^2 g^{-1}) and large pore volume (1.6 cm^3 g^{-1}), attributed to self-blowing and self-activating effects. This carbon foam was then coated with carbon nitride via wet impregnation with dicyandiamide (for either 1 or 24 hours) followed by thermal polymerisation, resulting in nitrogen contents of 5.3 at% (for C_3N_4/CF-1) and 17.0 at% (for C_3N_4/CF-24). However, the pore volume decreased to 1.3 and 0.8 cm^3 g^{-1}, respectively, attributed to the micropores being blocked and/or filled with carbon nitride. The three samples were investigated as adsorbents for CO_2 separation, and the key finding were as follows:

- At 100 kPa (relevant to post-combustion capture), coating with carbon nitride resulted in enhanced CO_2 uptake and selectivity compared to the uncoated carbon foam. This was attributed to a combination of the large micropore pore volume and increased isosteric heat of adsorption due to the introduction of Lewis base sites via nitrogen doping. However, higher nitrogen content resulted in lower CO_2 uptake due to the dramatically lower micropore volume.
- At 2 MPa (relevant to pre-combustion capture), coating with carbon nitride resulted in lower CO_2 uptake compared to the pure carbon foam. This was attributed to the increased importance of supermicropore and mesopore volume over nitrogen doping in this pressure regime.
- The regenerative capability of the adsorbents under pressure swing adsorption cycling displayed negligible deterioration over 15 tested cycles. This was attributed to the relatively weak adsorbate-adsorbent interactions and indicates the suitability of these unique adsorbents to be used in industrial applications.
- Furthermore, the adsorption characteristics of the materials presented in this work were competitive with the best results for carbon adsorbents reported in the literature, with a maximum adsorption capacity of ~25 mmol g^{-1}.

In summary, this study offers a nuanced understanding of CO_2 capture strategies via the use of novel materials with tailored properties. It emphasizes the potential application of alkoxide-derived carbon foams for pre-combustion capture technologies at high pressure. Furthermore, it underscores the benefit of tailoring nitrogen content to achieve selective CO_2 capture in post-combustion capture scenarios. This research advances our current understanding of adsorbents for CCS, offering new options for efficient operation across a wide spectrum of pressures and temperatures.

Acknowledgements

This work was supported by the Institute of Rock Structure and Mechanics, Czech Academy of Sciences (RVO: 67985891). M. Vorokhta gratefully acknowledges the Japan Society for the Promotion of Science (JSPS) for the financial support of the postdoctoral fellowship for research at Kyushu University, Japan (Fellow's ID: PE20030). M. I. M. Kusdhany acknowledges the JST, the establishment of university fellowships towards the creation of science technology innovation (Grant Number: JPMJFS2132). This work was also partially supported by JSPS KAKENHI Grant Number JP19H02558.

References

[1] NASA's Jet Propulsion Laboratory, California Institute of Technology, Understanding our planet to benefit humankind. Global Climate Chnage, Vital Sighns of the Planet., (n.d.). https://climate.nasa.gov/ (accessed October 13, 2023).

[2] K. Burrows, Climate Change - the science for everyone!, (n.d.). https://www.cs4s.net/climate-3.html (accessed October 13, 2023).

[3] R. Shaw, S. Naskar, T. Das, A. Chowdhury, A review on the advanced techniques used for the capturing and storage of CO_2 from fossil fuel power plants, in: Lect. Notes Civ. Eng., 2021: pp. 193-197.

[4] A. Mukherjee, J.A. Okolie, A. Abdelrasoul, C. Niu, A.K. Dalai, Review of post-combustion carbon dioxide capture technologies using activated carbon, J. Environ. Sci. (China) 83 (2019) 46–63.

[5] S.Y. Lee, S.J. Park, A review on solid adsorbents for carbon dioxide capture, J. Ind. Eng. Chem. 23 (2015) 1-11.

[6] M.E. Casco, M. Martínez-Escandell, J. Silvestre-Albero, F. Rodríguez-Reinoso, Effect

of the porous structure in carbon materials for CO_2 capture at atmospheric and high-pressure, Carbon 67 (2014) 230-235.

[7] M. Vorokhta, J. Morávková, D. Řimnáčová, R. Pilař, A. Zhigunov, M. Švábová, P. Sazama, CO_2 capture using three-dimensionally ordered micromesoporous carbon, J. CO_2 Util. 31 (2019) 124-134.

[8] M. Vorokhta, J. Nováková, M. Dopita, I. Khalakhan, V. Kopecký, M. Švábová, Activated three-dimensionally ordered micromesoporous carbons for CO_2 capture, Mater. Today Sustain. (2023) 100137.

[9] S. Licht, X. Liu, G. Licht, X. Wang, A. Swesi, Y. Chan, Amplified CO_2 reduction of greenhouse gas emissions with C2CNT carbon nanotube composites, Mater. Today Sustain. 6 (2019) 100023.

[10] V. Rahimi, A. Ferreiro-Salgado, D. Gómez-Díaz, M. Sonia Freire, J. González-Álvarez, Evaluating the performance of carbon-based adsorbents fabricated from renewable biomass precursors for post-combustion CO_2 capture, Sep. Purif. Technol. 344 (2024) 127110.

[11] A.R. Lieber, P. Boone, Y. He, J.A. Steckel, N.L. Rosi, C.E. Wilmer, K.M. Hornbostel, Parametric simulations of hierarchical core–shell MOF materials for direct air capture, Sep. Purif. Technol. 322 (2023) 124180.

[12] S. Ravi, Y. Choi, Y.S. Bae, Melamine-functionalized aromatic carbonyl-based polymer with high surface area for efficient CO_2 capture, Sep. Purif. Technol. 317 (2023) 123828.

[13] N. Chanchaona, C.H. Lau, Assessing the environmental impacts of flow and batch syntheses of hypercrosslinked polymers for low-pressure CO_2 adsorption, Sep. Purif. Technol. 329 (2024) 125145.

[14] A.M. Najafi, S. Soltanali, H. Ghassabzadeh, Enhancing the CO_2, CH_4, and N_2 adsorption and kinetic performance on FAU zeolites for CO_2 capture from flue gas by metal incorporation technique, Chem. Eng. J. 468 (2023) 143719.

[15] E. Aly, L.F.A.S. Zafanelli, A. Henrique, K. Gleichmann, A.E. Rodrigues, F.A. Da Silva Freitas, J.A.C. Silva, Separation of CO_2/N_2 in Ion-Exchange binder-free beads of zeolite NaY for Post-Combustion CO_2 capture, Sep. Purif. Technol. 348 (2024) 127722.

[16] N. Querejeta, M. V. Gil, F. Rubiera, C. Pevida, D. Wawrzyńczak, M. Panowski, I. Majchrzak-Kucęba, Bio-engineering of carbon adsorbents to capture CO_2 from industrial sources: The cement case, Sep. Purif. Technol. 330 (2024) 125407.

[17] V.K. Saini, M. Andrade, M.L. Pinto, A.P. Carvalho, J. Pires, How the adsorption properties get changed when going from SBA-15 to its CMK-3 carbon replica, Sep.

Purif. Technol. 75 (2010) 366-376.

[18] L. Liu, S. Jin, Y. Park, K.M. Kim, C.H. Lee, Sorption equilibria, kinetics, and temperature-swing adsorption performance of polyethyleneimine-impregnated silica for post-combustion carbon dioxide capture, Sep. Purif. Technol. 266 (2021) 118582.

[19] E.G. Al-Sakkari, A. Ragab, T.M.Y. So, M. Shokrollahi, H. Dagdougui, P. Navarri, A. Elkamel, M. Amazouz, Machine learning-assisted selection of adsorption-based carbon dioxide capture materials, J. Environ. Chem. Eng. 11 (2023) 110732.

[20] B. Dziejarski, J. Serafin, K. Andersson, R. Krzyżyńska, CO_2 capture materials: A review of current trends and future challenges, Mater. Today Sustain. 24 (2023) 100483.

[21] C.F. Martín, M.G. Plaza, J.J. Pis, F. Rubiera, C. Pevida, T.A. Centeno, On the limits of CO_2 capture capacity of carbons, Sep. Purif. Technol. 74 (2010) 225-229.

[22] H. Zhu, S. Li, J. Zhang, L. Zhao, Y. Huang, A highly effective and low-cost sepiolite-based solid amine adsorbent for CO_2 capture in post-combustion, Sep. Purif. Technol. 306 (2022) 122627.

[23] J. Serafin, B. Dziejarski, O.F. Cruz Junior, J. Sreńscek-Nazzal, Design of highly microporous activated carbons based on walnut shell biomass for H_2 and CO_2 storage, Carbon 201 (2022) 633-647.

[24] J. Luo, Y. Chen, H. Huang, R. Ma, N. Ma, F. Yan, J. Xu, J. Zhang, J. Chen, S. Sun, Microwave-coordinated KOH directionally modulated N/O co-doped porous biochar from Enteromorpha and its structure–effect relationships in efficient CO_2 capture, Chem. Eng. J. 473 (2023) 145279.

[25] J. Xiao, X. Yuan, T.C. Zhang, L. Ouyang, S. Yuan, Nitrogen-doped porous carbon for excellent CO_2 capture: A novel method for preparation and performance evaluation, Sep. Purif. Technol. 298 (2022) 121602.

[26] A. Rehman, G. Nazir, K. Yop Rhee, S.J. Park, A rational design of cellulose-based heteroatom-doped porous carbons: Promising contenders for CO_2 adsorption and separation, Chem. Eng. J. 420 (2021) 130421.

[27] A. Mukherjee, B. Saha, C. Niu, A.K. Dalai, Preparation of activated carbon from spent coffee grounds and functionalization by deep eutectic solvent: Effect of textural properties and surface chemistry on CO_2 capture performance, J. Environ. Chem. Eng. 10 (2022) 108815.

[28] M. Vorokhta, M.I.M. Kusdhany, D. Vöröš, M. Nishihara, K. Sasaki, S.M. Lyth, Microporous carbon foams: The effect of nitrogen-doping on CO_2 capture and separation via pressure swing adsorption, Chem. Eng. J. 471 (2023) 144524.

[29] S.M. Lyth, Y. Nabae, S. Moriya, S. Kuroki, M.A. Kakimoto, J.I. Ozaki, S. Miyata, Carbon nitride as a nonprecious catalyst for electrochemical oxygen reduction, J. Phys. Chem. C 113 (2009) 20148-20151.

[30] H. Liu, J. Liang, S. Fu, L. Li, J. Cui, P. Gao, F. Zhao, J. Zhou, N doped carbon quantum dots modified defect-rich g-C_3N_4 for enhanced photocatalytic combined pollutions degradation and hydrogen evolution, Colloids Surfaces A Physicochem. Eng. Asp. 591 (2020) 124552.

[31] Y. Oh, V.D. Le, U.N. Maiti, J.O. Hwang, W.J. Park, J. Lim, K.E. Lee, Y.S. Bae, Y.H. Kim, S.O. Kim, Selective and regenerative carbon dioxide capture by highly polarizing porous carbon nitride, ACS Nano 9 (2015) 9148-9157.

[32] C. Sathish, S. Premkumar, X. Chu, X. Yu, M.B.H. Breese, M. Al-Abri, A.H. Al-Muhtaseb, A. Karakoti, J. Yi, A. Vinu, Microporous carbon nitride ($C_3N_{5.4}$) with tetrazine based molecular structure for efficient adsorption of CO_2 and water, Angew. Chemie 133 (2021) 21412-21419.

[33] D.H. Park, K.S. Lakhi, K. Ramadass, M.K. Kim, S.N. Talapaneni, S. Joseph, U. Ravon, K. Al-Bahily, A. Vinu, Energy efficient synthesis of ordered mesoporous carbon nitrides with a high nitrogen content and enhanced CO_2 capture capacity, Chem. - A Eur. J. 23 (2017) 10753-10757.

[34] K.S. Lakhi, W.S. Cha, S. Joseph, B.J. Wood, S.S. Aldeyab, G. Lawrence, J.H. Choy, A. Vinu, Cage type mesoporous carbon nitride with large mesopores for CO_2 capture, Catal. Today. 243 (2015) 209-217.

[35] H.L. Peng, F.Y. Zhong, J.B. Zhang, J.Y. Zhang, P.K. Wu, K. Huang, J.P. Fan, L.L. Jiang, Graphitic carbon nitride functionalized with polyethylenimine for highly effective capture of carbon dioxide, Ind. Eng. Chem. Res. 57 (2018) 11031-11038.

[36] H. Li, M. Tang, X. Huang, L. Wang, Q. Liu, S. Lu, An efficient biochar adsorbent for CO_2 capture: Combined experimental and theoretical study on the promotion mechanism of N-doping, Chem. Eng. J. 466 (2023) 143095..

[37] I.M. Maulana Kusdhany, M. Kusdhany, Z. Ma, A. Mufundirwa, H. Li, K. Sasaki, A. Hayashi, M.S. Lyth, Hydrogen and carbon dioxide uptake on scalable and inexpensive microporous carbon foams, Microporous Mesoporous Mater. 343 (2022) 112141.

[38] S.M. Lyth, Carbon Foams in General, in: Nanocarbons Energy Convers. Supramol. Approaches, Springer International Publishing, 2019: pp. 175-203.

[39] E. Dautzenberg, S. van Hurne, M.M.J. Smulders, L.C.P.M. de Smet, GraphIAST: A graphical user interface software for Ideal Adsorption Solution Theory (IAST)

calculations, Comput. Phys. Commun. 280 (2022) 108494.

[40] G. Nazir, A. Rehman, S.J. Park, Self-activated, urea modified microporous carbon cryogels for high-performance CO_2 capture and separation, Carbon 192 (2022) 14-29.

[41] Y. Zhao, L. Wang, R. Malpass-Evans, N.B. McKeown, M. Carta, J.P. Lowe, C.L. Lyall, R. Castaing, P.J. Fletcher, G. Kociok-Köhn, J. Wenk, Z. Guo, F. Marken, Effects of g-C_3N_4 heterogenization into intrinsically microporous polymers on the photocatalytic generation of hydrogen peroxide, ACS Appl. Mater. Interfaces 14 (2022) 19938-19948.

[42] S.P. Pattnaik, A. Behera, S. Martha, R. Acharya, K. Parida, Facile synthesis of exfoliated graphitic carbon nitride for photocatalytic degradation of ciprofloxacin under solar irradiation, J. Mater. Sci. 54 (2019) 5726-5742.

[43] R.R. Mather, Surface modification of textiles by plasma treatments, Surface Modification of Textiles, Woodhead Publishing Limited, 2009: pp. 296-317.

[44] G.J. Hutchings, P.R. Davies, S. Pattisson, T.E. Davies, D.J. Morgan, M.W. Dlamini, Facile synthesis of a porous 3D g-C3N4 photocatalyst for the degradation of organics in shale gas brines, Catal. Commun. 169 (2022) 106480.

[45] B.H.S. Felipe, R.L.B. Cabral, R. Ladchumananandasivam, A. Zille, S. Kim, P.B.A. Fechine, J.H.O. Nascimento, Nanocoating on cotton fabric with nitrogen-doped graphene quantum dots/titanium dioxide/PVA: An erythemal UV protection and photoluminescent finishing, J. Mater. Res. Technol. 18 (2022) 2435-2450.

[46] I.H. Tseng, Y.M. Sung, P.Y. Chang, C.Y. Chen, Anatase TiO_2 - decorated graphitic carbon nitride for photocatalytic conversion of carbon dioxide, Polymers (Basel). 11 (2019) 1-16.

[47] P. Liu, N. Sun, Y. Liang, F. Chen, Modified graphitic carbon nitride prepared via a copolymerization route for superior photocatalytic activity, Res. Chem. Intermed. 44 (2018) 843-857.

[48] A. Kumar, P. Kumar, C. Joshi, M. Manchanda, R. Boukherroub, S.L. Jain, Nickel decorated on phosphorous-doped carbon nitride as an efficient photocatalyst for reduction of nitrobenzenes, Nanomaterials 6 (2016) 59.

[49] J. Liu, D. Takeshi, K. Sasaki, S.M. Lyth, Platinum-decorated nitrogen-doped graphene foam electrocatalysts, Fuel Cells 14 (2014) 728-734.

[50] A.C. Ferrari, Raman spectroscopy of graphene and graphite: Disorder, electron–phonon coupling, doping and nonadiabatic effects, Solid State Commun. 143 (2007) 47-57.

[51] Serafin, J., Dziejarski, B. Activated carbons – preparation, characterization and their application in CO_2 capture: A review, Environ. Sci. Pollut. Res. 31 (2024) 40008-40062.

[52] G. Singh, K. Ramadass, J.M. Lee, I.S. Ismail, M. Singh, V. Bansal, J.H. Yang, A. Vinu, Convenient design of porous and heteroatom self-doped carbons for CO_2 capture, Microporous Mesoporous Mater. 287 (2019) 1-8.

[53] A. Silvestre-Albero, J. Silvestre-Albero, M. Martinez-Escandell, M. Molina-Sabio, A. Kovacs, F. Rodriguez-Reinoso, Novel synthesis of a micro-mesoporous nitrogen-doped nanostructured carbon from polyaniline, Microporous Mesoporous Mater. 218 (2015) 199-205.

[54] B.C. Lippens, J.H. de Boer, Studies on pore systems in catalysts: V. The t method, J. Catal. 4 (1965) 319-323.

[55] X. Liu, S. Wang, C. Sun, H. Liu, L. Stevens, P.K. Dwomoh, C. Snape, Synthesis of functionalized 3D microporous carbon foams for selective CO_2 capture, Chem. Eng. J. 402 (2020) 125459.

[56] X. Peng, Y.L. Peng, M. Huo, J. Zhao, Q. Ma, B. Liu, C. Deng, M. Yang, B. Dong, C. Sun, G. Chen, High efficient pre-combustion CO_2 capture by using porous slurry formed with ZIF-8 and isoparaffin C16, Sep. Purif. Technol. 305 (2023) 122424.

[57] S. Dantas, K.C. Struckhoff, M. Thommes, A. V. Neimark, Pore size characterization of micro-mesoporous carbons using CO_2 adsorption, Carbon 173 (2021) 842-848.

[58] H. Cui, J. Xu, J. Shi, S. You, C. Zhang, N. Yan, Y. Liu, G. Chen, Evaluation of different potassium salts as activators for hierarchically porous carbons and their applications in CO_2 adsorption, J. Colloid Interface Sci. 583 (2021) 40-49.

[59] J. Shi, N. Yan, H. Cui, J. Xu, Y. Liu, S. Zhang, Salt template synthesis of nitrogen and sulfur co-doped porous carbons as CO_2 adsorbents, ACS Sustain. Chem. Eng. 7 (2019) 19513-19521.

[60] Y.-C. Chiang, C.-Y. Wu, Y.-J. Chen, Effects of activation on the properties of electrospun carbon nano fibers and their adsorption performance for carbon dioxide, Sep. Purif. Technol. 233 (2020) 116040.

[61] H.S. Kim, M.S. Kang, S. Lee, Y.W. Lee, W.C. Yoo, N-doping and ultramicroporosity-controlled crab shell derived carbons for enhanced CO_2 and CH_4 sorption, Microporous Mesoporous Mater. 272 (2018) 92-100.

[62] D.J. Tao, F.F. Mao, J.J. Luo, Y. Zhou, Z.M. Li, L. Zhang, Mesoporous N-doped carbon derived from tea waste for high-performance CO_2 capture and conversion, Mater. Today Commun. 22 (2020) 100849.

[63] F. Liu, K. Huang, S. Ding, S. Dai, One-step synthesis of nitrogen-doped graphene-like meso-macroporous carbons as highly efficient and selective adsorbents for CO_2 capture,

J. Mater. Chem. A 4 (2016) 14567-14571.

[64] G. Chandrasekar, W.J. Son, W.S. Ahn, Synthesis of mesoporous materials SBA-15 and CMK-3 from fly ash and their application for CO_2 adsorption, J. Porous Mater. 16 (2009) 545-551.

[65] H.M. Coromina, D.A. Walsh, R. Mokaya, Biomass-derived activated carbon with simultaneously enhanced CO_2 uptake for both pre and post combustion capture applications, J. Mater. Chem. A 4 (2015) 280-289.

[66] V. Goetz, O. Pupier, A. Guillot, Carbon dioxide-methane mixture adsorption on activated carbon, Adsorption 12 (2006) 55-63.

[67] D. Cazorla-Amorós, J. Alcañiz-Monge, M.A. de la Casa-Lillo, A. Linares-Solano, CO_2 as an adsorptive to characterize carbon molecular sieves and activated carbons, Langmuir 14 (1998) 4589-4596.

[68] W. Zhu, Y. Wang, F. Yao, X. Wang, H. Zheng, G. Ye, H. Cheng, J. Wu, H. Huang, D. Ye, One-pot synthesis of N-doped petroleum coke-based microporous carbon for high-performance CO_2 adsorption and supercapacitors, J. Environ. Sci. (China) 139 (2024) 93-104.

[69] T. Guo, Y. Zhang, J. Chen, W. Liu, Y. Geng, A.H. Bedane, Y. Du, Investigation of CO_2 adsorption on nitrogen-doped activated carbon based on porous structure and surface acid-base sites, Case Stud. Therm. Eng. 53 (2024) 103925.

[70] S. He, G. Chen, H. Xiao, G. Shi, C. Ruan, Y. Ma, H. Dai, B. Yuan, X. Chen, X. Yang, Facile preparation of N-doped activated carbon produced from rice husk for CO_2 capture, J. Colloid Interface Sci. 582 (2021) 90-101.

[71] Q. Li, S. Liu, L. Wang, F. Chen, J. Shao, X. Hu, Efficient nitrogen doped porous carbonaceous CO_2 adsorbents based on lotus leaf, J. Environ. Sci. (China) 103 (2021) 268-278.

[72] S. Shingdilwar, S. Dolui, D. Kumar, S. Banerjee, Facile access to template-shape-replicated nitrogen-rich mesoporous carbon nanospheres for highly efficient CO_2 capture and contaminant removal, Mater. Adv. 3 (2022) 665-671.

[73] L. Vazhayal, P. Wilson, K. Prabhakaran, Utilization of waste aquatic weeds for the sustainable production of nitrogen doped nanoporous carbon for CO_2 capture, Mater. Today Proc. 52 (2021) 2315-2321.

[74] S. Zhou, C. Guo, Z. Wu, M. Wang, Z. Wang, S. Wei, S. Li, X. Lu, Edge-functionalized nanoporous carbons for high adsorption capacity and selectivity of CO_2 over N_2, Appl. Surf. Sci. 410 (2017) 259-266.

[75] J. Li, W. Zhou, Y. Huang, Y. Zhao, X. Li, N. Xue, Z. Qu, Z. Tang, L. Xie, X. Meng, J. Gao, F. Sun, P. Wang, X. Pi, G. Zhao, Y. Qin, Rapid, simple and sustainable preparation of N-rich activated carbons with high performance for gas adsorption, via microwave heating, Sep. Purif. Technol. 330 (2024) 125464.

[76] L.M. Esteves, T.J. Ferreira, A. Keba, J.M.S.S. Esperança, I.A.A.C. Esteves, Carbon materials derived from cyano-based IL@ZIF-8 composites for CO_2 sorption separation systems, Mater. Today Sustain. 22 (2023) 100353.

[77] X. Wu, J.Y. Zhang, L. Sen Zhou, R. Guan, W.T. Zheng, Z.Q. Tian, K. Huang, F. Liu, Graphene-based mesoporous frameworks with ultrahigh nitrogen contents for highly efficient and selective sulfur dioxide capture, Chem. Eng. J. 412 (2021) 128677.

[78] E. Gomez-Delgado, G. Nunell, A.L. Cukierman, P. Bonelli, Tailoring activated carbons from Pinus canariensis cones for post-combustion CO_2 capture, Environ. Sci. Pollut. Res. (2020). doi:10.1007/s11356-020-07830-4.

[79] C. Goel, H. Bhunia, P.K. Bajpai, Mesoporous carbon adsorbents from melamine-formaldehyde resin using nanocasting technique for CO_2 adsorption, J. Environ. Sci. (China) 32 (2015) 238-248.

[80] M. Balsamo, A. Silvestre-Albero, J. Silvestre-Albero, A. Erto, F. Rodríguez-Reinoso, A. Lancia, Assessment of CO_2 adsorption capacity on activated carbons by a combination of batch and dynamic tests, Langmuir 30 (2014) 5840-5848.

[81] K. Huang, Z.L. Li, J.Y. Zhang, D.J. Tao, F. Liu, S. Dai, Simultaneous activation and N-doping of hydrothermal carbons by $NaNH_2$: An effective approach to CO_2 adsorbents, J. CO_2 Util. 33 (2019) 405-412.

[82] V.V. Karve, J. Espín, M. Asgari, S. Van Gele, E. Oveisi, W.L. Queen, N-containing carbons derived from microporous coordination polymers for use in post-combustion flue gas capture, Adv. Funct. Mater. 33 (2023) 2212283.

[83] D. Saha, S.E. Van Bramer, G. Orkoulas, H.C. Ho, J. Chen, D.K. Henley, CO_2 capture in lignin-derived and nitrogen-doped hierarchical porous carbons, Carbon 121 (2017) 257-266.

[84] P. Ammendola, F. Raganati, R. Chirone, CO_2 adsorption on a fine activated carbon in a sound assisted fluidized bed: Thermodynamics and kinetics, Chem. Eng. J. 322 (2017) 302-313.

[85] J. Serafin, B. Dziejarski, X. Vendrell, K. Kiełbasa, B. Michalkiewicz, Biomass waste fern leaves as a material for a sustainable method of activated carbon production for CO_2 capture, Biomass and Bioenergy 175 (2023) 106880.

[86] A. Rehman, S.J. Park, From chitosan to urea-modified carbons: Tailoring the ultra-microporosity for enhanced CO_2 adsorption, Carbon 159 (2020) 625-637.

[87] E. Maruccia, A. Piovano, M.A.O. Lourenço, T. Priamushko, M. Cavallo, S. Bocchini, F. Bonino, F.C. Pirri, F. Kleitz, C. Gerbaldi, Revealing the competitive effect of N_2 and H_2O towards CO_2 adsorption in N-rich ordered mesoporous carbons, Mater. Today Sustain. 21 (2023) 100270.

[88] Y. Wang, J. Xu, X. Lin, B. Wang, Z. Zhang, Y. Xu, Y. Suo, Facile synthesis of MOF-5-derived porous carbon with adjustable pore size for CO_2 capture, J. Solid State Chem. 322 (2023) 123984.

[89] M.G. Plaza, S. García, F. Rubiera, J.J. Pis, C. Pevida, Post-combustion CO_2 capture with a commercial activated carbon: Comparison of different regeneration strategies, Chem. Eng. J. 163 (2010) 41-47.